

# **SIMMER code Two-Fluid Model Well-posedness and Stability for simulating Liquid Metal (Lead-Lithium Eutectic), water vapor, and non-condensable gases multi-component multi-phase flows**

**Satya Prakash Saraswat<sup>1\*</sup>, Nicola Forgone<sup>1</sup>**

<sup>1</sup>Laboratory of Numerical Simulations for Nuclear Thermal-Hydraulics  
Department of Civil and Industrial Engineering, University of Pisa, Pisa Italy, 56122  
[satya.saraswat@ing.unipi.it](mailto:satya.saraswat@ing.unipi.it)

\*Correspondence: [satya.saraswat@ing.unipi.it](mailto:satya.saraswat@ing.unipi.it); Tel.: (+39-3313486219)

## **Abstract**

Liquid metals are employed as a coolant in liquid metal fast reactors (LMFR) and are considered breeders and coolants for future power-producing fusion reactors. The interaction of liquid metals with other coolants, such as air and water, is one of the possible occurrences in liquid metal-cooled reactors. Although the SIMMER-III computer code is currently in the validation and verification phase, it is a prospective candidate code for correctly investigating possible accidents. This study aims to determine the stability and well-posedness of the SIMMER-III code Eulerian-Eulerian two-fluid model (TFM) under any such accident scenario. This work also considers the influence of the virtual mass force and diffusion forces in momentum on TFM stability in accelerated liquid metal, steam, and non-condensable gaseous flows throughout all flow regimes. The characteristics method is used to assess the ill-posed nature of TFM for all types of accidents and accident scenarios in a hypothetical simplified system model with several components (Lead-Lithium, non-condensable gases, and water vapor). It has been discovered that the analysis findings vary from the air and water two-component two-phase flows (characteristics roots spectrum and error growth rate patterns) and are particularly sensitive to the diffusion and virtual mass coefficients. This is because liquid metals have a higher density than liquid water and steam, resulting in strong virtual mass forces and weak diffusion forces in liquid-metal and gas two-phase flows. Because of the extensive range of possible interactions between fluxes of different components, producing an accurate representation of diffusion in multi-component mixtures is difficult. Because of this, it is strongly suggested that the virtual mass coefficient and diffusion coefficients be handled more accurately for these kinds of flows. The values of these coefficients significantly affect how accurate proposed TFM predictions are, but there hasn't been much research on how to estimate them. The study also sheds light on the model's accuracy and highlights the areas where the model's predictions will be mathematically trustworthy.

## **Keywords**

Liquid-metals; Two fluid model; Liquid-Metal and Non-condensable gas flow; Eigenvalue analysis; Linear stability, thermal-hydraulics; two-phase flow

## **Highlights**

- Check the ill-posed nature of the two-component-two-phase (Liquid lead-lithium eutectic, steam, and non-condensable gases) mixture flow model of SIMMER code.
- The adjusted by changing numerous flows and heat transfer factors (pressure, void fraction, phasic velocities, slip ratio, non-condensable quality, diffusion coefficient, and coefficient of closure correlations of phasic momentum transfer equations) on the ill-posedness of the continuity equations is investigated.
- Explain the system's mathematical characteristics used in Liquid-metal and gas two-phase flow modeling.

## 1. Introduction:

System codes are essential in thermal-hydraulic simulations of nuclear reactors and other multi-phase systems. The governing equations for most system codes are formulated with the two-fluid model (Eulerian-Eulerian) approach. Since its origin, the ill-posed nature of the two-fluid model (TFM) to simulate the two-phase flow phenomenon has been a classical problem [1-7]. The model's Well-posedness is necessary but not the least condition to confirm that the simulation results produced by this model are accurate and reliable [4-7]. Much research has been performed to make such models well-posed for a variety of fluids and thermodynamic conditions. However, the characteristics of the TFM are highly dependent on the fluid properties and the flow conditions. Therefore, there is no unique approach to make the model well-posed [1-3]. Therefore, it is always required to perform the mathematical analysis of TFM for different fluids, and the various fluids flow conditions to find the optimized way to make the model well-posed without costing the computational accuracy and speed.

The utilization of heavy liquid metals is rapidly rising in numerous scientific domains and industries [8 and 9]. A thorough understanding of the underlying thermal-hydraulic processes associated with their utilization is required to build numerical codes utilized in R&D and engineering design of liquid metal components. Liquid metals are a type of coolant with a high thermal conductivity, which means they have better heat transfer coefficients for the same flow characteristics [8]. Liquid metals are distinguished by their low vapor pressure, which allows them to operate high-temperature engineering equipment at reduced pressure without reducing mechanical hardness [8-11].

In Liquid Metal fast reactors (LMFR) and future power-producing fusion reactors [10-11], multiple fluids (Liquid Metal, Water, and Non-condensable gases) are employed to extract heat from the reactor secondary side of the heat-exchanger. One of the best examples of multi-fluid coolant reactors is the experimental fusion reactor (ITER) [12]. Multiple fluid interactions are possible in these types of reactors under the identified distinct accident scenarios. Although these reactors are rather robust in nature and the possibility of an accident is low, high accuracy thermal and hydraulic protection evaluations are required to prevent accidents [11-13].

Because deterministic safety assessment has always been undertaken throughout various phases of the licensing and functionality processes, mathematical modeling and computer simulation play a critical role in nuclear power plant safety [1-3]. As a result, a thorough grasp of various modeling methodologies is required. Moreover, because most of today's thermal hydraulics system codes were created between the 1970s and 1990s [1-6], there is a need to revisit the modeling techniques used by these codes, particularly now when a variety of computationally intensive tools are established that can offer a broad range of applications and make mathematical investigations relatively easy [4]. In the generation IV reactors and DEMO fusion reactor systems [11 and 12], the liquid metal coolant has introduced the new challenge for accurately modeling the accident scenarios with the existing codes [10 and 11]. With some modifications, the existing codes are going to be applied, but the basic structure of modeling fluid flow and heat transfer conservation equation remains the same.

The existence of liquid metals in the liquid phase and the non-condensable gases in the vapor phase (such as hydrogen due to chemical reactivity of liquid metals with water and air from the surrounding environment) in the two-phase flows results in the complex multi-component two-phase flow modeling [12 and 13]. To accurately perform such simulations by using these codes, the mathematical nature of the modeling equations must be accessed for such new fluids and complex fluid conditions, which are highly unknown and can severely impact the simulation results.

It is critical to have an accurate estimate of transient two-phase multi-component flow when doing safety evaluations on nuclear reactors during design base accident situations [1-3]. Because of the reactor shape and the likelihood of transient two-phase flow, the fluid flow and heat transfer that must be dealt with are sometimes quite complicated, especially in liquid-metal and non-condensable gas mixture flow [13]. A blending of comprehensive model building, robust computational tools, and a variety of small as well as large validating investigations has recently resulted in significant advancements in the interpretation and prediction of these physical processes. There is still no past study on the stability of liquid-metal and non-condensable two-component two-phase flow models.

Still, there has been a lot of extensive research on TFM stability for water and two-phase air flow over the last 50 years, which has been used in this paper to determine the sample fluid conditions that will lead to the non-hyperbolic nature of liquid-metal vapor and non-condensable two-component two-phase flow models. In the following paragraph, a brief literature overview of two-fluid model stability for air-water two-phase flow is described to grasp the current state of the art of TFM stability methods and regularization approaches and their benefits drawbacks.

One of the most recent works [1, 2 and 3] comprehensively examines and understands thermal-hydraulic system codes underlying TFM and the theoretically simple set of conservation laws. These studies focus on diffusion and the bubble collision force for dispersed two-phase flows and offer eigenvalue evaluation, linear instability assessment, Von-Neumann computational stability analysis, and regularization. In their most recent scientific article, Fullmer et al. [4] examined the linear stability of SIMMER-III TFM. On the other hand, the system codes model does not explicitly resolve those equations, instead of solving the computational convenience set of equations, which reduces the study's accuracy in this report. Ramshaw and Trapp [5] investigated the characteristics, stability, and high-frequency phenomena of two-phase flow equation systems. They demonstrated that instability occurs only when the wavelength of the disturbance appears to be zero. This research contributes to our understanding of TFM's possible short-wavelength volatility. The two-phase simulation convergence and accuracy expectations are the subjects of Ransom et al. [6]. This paper provides insight into convergence approaches and aids in the understanding of numerical uncertainty. Lyczkowski et al. [7] attempted to demonstrate the dynamic properties of most two-phase flow models for two-phase steam-water systems in some priority areas. This document can assist in locating complex features. It is inextricably tied to the analyses offered in the current paper. Weisman et al. [14] show how to use the characteristic equation to identify non-hyperbolic regions in the governing equation set, removing physically implausible patterns and chaotic solutions. Lim et al. [15] presented MARS with the details of hyperbolic two-fluid equations. They recommended that an interfacial pressure force term be included in the conservation equations to improve the system's hyperbolic and numerical stability.

As per the present state of the art, the virtual mass force and diffusion forces are significant phenomenon that must be considered when modeling two-phase flows with TFM to ensure that the model is well-posed. For liquid-metal and gas two-phase flow, Satyamurthy et al. [16] used a two-fluid model. The Runge–Kutta method was used to numerically solve one-dimensional steady-state two-fluid flow equations with each phase's mass, momentum, and auxiliary relations. Usov et al. [17] go over all the relationships and numerical methods for simulating gas-phase transport in a vertical liquid metal column in detail.

The foundation of two-phase-flow models for liquid-metal (lead-lithium) and gas and their restrictions due to ill-posedness are examined in this work based on the well-developed model for air-water TFM the critical relevance of these models [18-20]. The effect of well-established forces in phasic momentum equations like diffusion and virtual mass forces on the well-posedness of the liquid-metal and air two-phase flow is also identified under this study for large flow patterns and tested for simplified WCLL TBS like environments [12]. Based on the analysis, modification in the reference TFM is suggested, and extra efforts are needed to find the critical coefficients and correlations accurately due to their high sensitivity for such applications.

It is well established that lithium-lead is exceptionally reactive to the water, and the reaction is exothermic, and hydrogen is produced in the reaction outcome, which can disturb the flow in the system [13]. And even if the energy is released in the slight reaction, that can only change the energy conservation equation, which is also considered as a heated column. The consideration of hydrogen produced in the exothermic reaction can only change the non-condensable gas fraction [13], which is also considered in the presented analysis. However, in the current analysis, the assumption is that in a channel, lithium-lead is in the liquid phase, and the air, which is relatively non-reactive and water vapors are in small fraction at a low temperature, so the lithium, water vapor and the non-condensable gases flow is possible without or a slight chemical reaction at least for a short period of time and at a lower temperature. A similar model is also taken in literature [16 and 17] before for the air and lithium lead.

Several thermal-hydraulic safety analysis algorithms are available to study two-fluid interactions (Liquid-Metal, water, and non-condensable gases) with their thermal-hydraulic characteristics. ASYST, SIMMER, and MELCOR are prospective candidate system codes for simulating the thermal-hydraulic spectrum of liquid metals, water, and non-condensable gases [3,12 and 13]. We employ the SIMMER-III based conservation equations for fluid flow in this research because they have been used for fifty years. Many other codes (MELCOR, ASYST) use the same system of equations with minor adjustments, which do not affect the root spectrum properties. These equations have been thoroughly proven via extensive tests in light water thermal-hydraulics. Adjustments for a new fluid (Lead-Lithium) may be used to forecast the thermodynamics of Liquid-Metal and gas two-phase flows accurately.

The usefulness of the numerical solutions to the two-phase flow concerns with complex TFM features in nuclear reactor safety evaluation was explored in this paper. This paper's analysis is for a multi-component, two-phase flow of Liquid Metal, water vapor, and non-condensable gases. The research is carried out in a MATLAB environment. According to the study, in some of the sample fluid conditions under the transient to accident scenario, the differential equations being solved had complex roots, resulting in an ill-posed problem. The importance of virtual mass force and diffusion factors in momentum equations in predicting the thermal-hydraulic spectrum of multi-component, two-phase flow is proven, implying that precise closure relation coefficients are required for simulations of such flow features.

## **2 Lead-Lithium, non-condensable and steam two-phase-multi-component flow modeling methodology in SIMMER-III**

SIMMER-III is a two-dimensional, three-velocity-field, multiphase, multi-component, Eulerian, thermal-hydraulic computer code with a space- and energy-dependent neutron dynamics model [13]. This code can be utilized for up to 27 density components and 16 energy components, respectively. Mass and energy conservation equations are solved to represent complex flow circumstances in a postulated accident scenario. Lead-Lithium, non-condensable and water-steam two-phase-multi-component flow model consider for the present analysis is based on the conservation equations of SIMMER [13] and utilize the equations with little modification for simplification by avoiding some algebraic terms, which does not affect the mathematical characteristics of the system of governing equations [7]. The model considered is based on a multi-fluid, 2-dimensional model of multi-phase flows. Separate conservation equations for mass, momentum, and energy are written in this model for the liquid and vapor and gas components. For inter-phase transport of mass, momentum, and energy, constitutive relationships are defined. Heat transfer between fluids and passive materials like pipe walls can be modeled. There are also models for wall friction and two-phase critical flow. The liquid phase is considered for water and liquid Lead-Lithium eutectic and the gas phase is considered for steam and non-condensable gases like air and hydrogen in present analysis. These equations consist of 6 mass conservation equations (one for lead-lithium liquid and phase, two for water and three for non-condensable gases (air and hydrogen)), similarly the model corresponds 3 momentum equations (one for liquid water velocity component, one for liquid lead-lithium velocity component and third for the vapor and non-condensable gases combined velocity components) and six energy conservation equations for different components as discussed above.

Constitutive correlations are used to close the mathematical model, including state-of-the-art mathematical model for interfacial mass transport, interfacial forces, liquid, and water vapor wall thrust, wall and surface heat exchange, and the thermodynamic properties of lead-lithium eutectic, steam, and non-condensable gases.

The original SIMMER-III equations are available in literatures [21,22 and 23] and a simplified version of these equations for lead-lithium, steam, and non-condensable two-phase-multi-component flow with addition of diffusion forces are given here for convenience.

In SIMMER-III, conservation equations are written for independent variables in a unit volume. Thus, the mass and energy are represented by macroscopic density and specific

internal energy, respectively. The conservation equations involving fluid mass, momentum and internal energy are, in abbreviated form:

$$\frac{\partial \bar{\rho}_m}{\partial t} + \nabla \cdot (\bar{\rho}_m v_q) = -\Gamma_m \dots \dots (1)$$

$$\frac{\partial \bar{\rho}_q v_q}{\partial t} + \sum_{m \in q} \nabla \cdot (\bar{\rho}_m v_q v_q) + \alpha_q \nabla p - \bar{\rho}_q g + K_{qs} v_q - \sum_{q'} K_{qq'} (v_{q'} - v_q) - VM_q = -\sum_{q'} \Gamma_{qq'} [H(\Gamma_{qq'}) v_q + H(-\Gamma_{qq'}) v_{q'}] \dots \dots (2)$$

$$\frac{\partial \bar{\rho}_M e_M}{\partial t} + \sum_{m \in M} \nabla \cdot (\bar{\rho}_m e_m v_q) + p \left[ \frac{\partial \alpha_m}{\partial t} + \nabla \cdot (\alpha_m v_q) \right] - \frac{\bar{\rho}_M}{\bar{\rho}_m} \left[ \sum_{q'} k_{q'q} (v_q - v_{q'}) \cdot (v_q - v_{q'}) + K_{qs} v_q \cdot (v_q - v_{qs}) - VM_q \cdot (v_q - v_{GL}) \right] = Q_N + Q_M(\Gamma_m) + Q_H(h, a, \Delta T) \dots \dots (3)$$

In the above equations, the density components are subscripted by  $m$ , the energy components by  $M$ , the velocity components by  $q$ , primary variables are component densities, energy and pressure. For the case under study which involves 6 components that can affect the flow characteristics (lead-lithium eutectic, liquid water, steam, hydrogen, argon gas and air) so here  $m=6$ , three separate velocities for each field (liquid, vapor, and non-condensable gases) so  $q=3$ . For the simplification and as per the environmental conditions for the current case of analysis we only consider two-velocities and assume that the liquid lead-lithium velocity is zero. So, for the case studied in this research paper, there are 6 mass conservation equations for each component, two momentum equations for two phases of fluid (liquid and vapour), six energy conservation equations (one for each component).

Since the component specific densities ( $\rho_m$ )/volumes( $\vartheta_m$ ) (not microscopic densities/volume) are used in the SIMMER-III EOS model, macroscopic densities  $\bar{\rho}_m$  are related to volume fractions  $\alpha_m$  by equation (4)

$$\alpha_m = \bar{\rho}_m \vartheta_m \dots (4)$$

Or the relationship to microscopic densities to specific densities are given by equation (5)

$$\bar{\rho}_m = \alpha_m \rho_m \dots (5)$$

Also, the sum of all volume fractions of the component for the close system is equals to one and defined in by equation (6)

$$\sum_{n=1}^m \alpha_m = 1 \dots \dots (6)$$

So, from equation 6 we can reduce the one extra redundant void fraction variable, therefore the void fraction variables utilized in the analysis is ‘ $m-1$ ’ which is 5 in the analysis presented here although in wider sense it is reduced to 1 which is void fraction of vapor phase. And the specific densities can be written in terms of system pressure  $P$  and the internal energies  $e_M$ .

$$\partial \rho_m = \left( \frac{\partial \rho_m}{\partial P} \right) \partial P + \left( \frac{\partial \rho_m}{\partial e_m} \right) \partial e_m \dots \dots (7)$$

$$\alpha_m \left( \frac{\partial \rho_m}{\partial P} \right) \frac{\partial P}{\partial t} + \alpha_m \left( \frac{\partial \rho_m}{\partial e_m} \right) \frac{\partial e_m}{\partial t} + (\rho_m) \frac{\partial \alpha_g}{\partial t} + \alpha_m v_q \left( \frac{\partial \rho_m}{\partial P} \right) \frac{\partial P}{\partial x} + \alpha_m v_q \left( \frac{\partial \rho_m}{\partial e_m} \right) \frac{\partial e_m}{\partial x} + \alpha_m \rho_m \frac{\partial v_q}{\partial x} + \rho_m v_q \frac{\partial \alpha_m}{\partial x} = -\Gamma_m \dots (8)$$

$$\alpha_m \rho_m \frac{\partial v_q}{\partial t} + \sum_{m \in q} \alpha_m \rho_m \frac{\partial v_q^2}{\partial x} + \alpha_q \frac{\partial P}{\partial x} - \alpha_q \rho_q g + K_{qs} v_q - \sum_{q'} K_{qq'} (v_{q'} - v_q) - VM_q = -\sum_{q'} \Gamma_{qq'} [H(\Gamma_{qq'}) v_q + H(-\Gamma_{qq'}) v_{q'}] \dots (9)$$

$$\begin{aligned} & (\rho_m e_m + P) \frac{\partial \alpha_m}{\partial t} + \alpha_m e_m \frac{\partial \rho_m}{\partial t} + \alpha_m \rho_m \frac{\partial e_m}{\partial t} + \alpha_g v_q e_m \left( \frac{\partial \rho_g}{\partial P} \right) \frac{\partial P}{\partial x} + \alpha_m v_q e_m \left( \frac{\partial \rho_m}{\partial e_m} \right) \frac{\partial e_m}{\partial x} \\ & + \alpha_m v_q \rho_m \frac{\partial e_m}{\partial x} + v_q \rho_m e_m \frac{\partial \alpha_m}{\partial x} + \rho_m e_m \alpha_m \frac{\partial v_q}{\partial x} + P \alpha_m \frac{\partial v_q}{\partial x} + P v_q \frac{\partial \alpha_m}{\partial x} \\ & + VM_q (v_q - v_{GL}) - \frac{\bar{\rho}_M}{\rho_m} \left[ \sum_{q'} k_{q'q} (v_q - v_{q'}) \cdot (v_q - v_{q'}) + K_{qs} v_q (v_q - v_{qs}) \right] \\ & = Q_N + Q_M(\Gamma_m) + Q_H(h, a, \Delta T) \dots (10) \end{aligned}$$

Therefore, to analyze the system mathematical we have total 14 primary dependent variables (1 volume fractions quality factor, X that define different components, 2 specific internal energies, 2 velocities and 1 system pressure). Although these primary variables can be further reduced to 7 by considering that only two volume fractions (one for liquid phase  $\alpha_l$  one for gaseous phase  $\alpha_g$ ), two combine internal energies (one for liquid phase  $e_l$  one for gaseous phase  $e_g$ ) that are sufficient to define the system characteristics.

## 2.1 Physical Property Data for Fluids

The thermodynamic and transport properties of the fluids are needed to determine the two-phase flow characteristics. These properties are required for single-phase liquids, single-phase vapors, and saturated vapor/liquid mixtures. As a function of absolute pressure, the following thermodynamic properties are required:

1. Saturation temperature
2. Specific heat for gas and liquid phases
3. Thermal expansion coefficient for gas and liquid phases
4. Isothermal compressibility for gas and liquid phases
5. Specific volume/density for gas and liquid phases
6. Specific internal energies for gas and liquid phases.

These physical properties for water and non-condensable gases are widely available in various literatures.

The correlations for thermo-dynamic and physical properties of lithium-lead are taken from various published articles [24-31] and are listed below. The literature [24] gives a summary of isobaric and isothermal compressibility variables utilized in the investigation.

The liquid lead-lithium eutectic density, specific heat and internal energy are given by equations (11), (12) and (13)

$$\rho_{pbli} = 10520.35 - 1.19051 * T \quad (11)$$

$$C_{P pbli} = 195 - 9.116 * 10^{-3} * T \quad (12)$$

$$u_{pbli} = 195 * T - \frac{0.009116 * T^2}{2} \quad (13)$$

The isobaric compressibility of liquid metal (lead lithium eutectic)  $\beta_f$ , steam  $\beta_s$  and non-condensable gases  $\beta_n$  and total gaseous phase isobaric compressibility  $\beta_g$  are mentioned below in equations (14), (15), (16) and (17) respectively

$$\beta_f = \frac{1}{\rho_f} \left( \frac{\partial \rho_f}{\partial T_f} \right)_P = (11.221 + 1.531 * 10^{-3}T) * 10^{-5} \dots \dots \dots (14)$$

$$\beta_s = \frac{1}{\rho_s} \left( \frac{\partial \rho_s}{\partial T_g} \right)_P \dots \dots \dots (15)$$

$$\beta_n = \frac{1}{\rho_n} \left( \frac{\partial \rho_n}{\partial T_g} \right)_P = \frac{1}{T_g} \dots \dots \dots (16)$$

$$\beta_g = \frac{1}{\rho_g} \left( \frac{\partial \rho_g}{\partial T_g} \right)_P = \frac{1}{\rho_g} [\rho_s \beta_s + \rho_n \beta_n] \dots \dots (17)$$

Here  $\beta_s$  represents the isobaric compressibility of water vapor as the isobaric compressibility for lithium-lead vapors are negligible compared to water vapors,  $\beta_f$  represents the isobaric compressibility of liquid (lead lithium eutectic) phase,  $\beta_n$  represents the isobaric compressibility of non-condensable gas, T represents temperature, and P represents pressure.

In the same way, we discovered compressibility in an isothermal condition. Equations (18), (19), (20) and (21) show the isothermal compressibility of liquid metal (lead lithium eutectic)  $k_f$ , steam  $k_s$ , non-condensable gases  $k_n$ , and total gaseous phase  $k_g$  respectively.

$$\text{for liquid metal } k_{fLM} = \frac{-1}{\rho_f} \left( \frac{\partial \rho_f}{\partial P} \right)_{T_f} = \frac{1}{(1876 - 306T(^{\circ}\text{C}))^2 * \rho_f} + \frac{T(K) * \beta_f^2}{\rho_f * C_p} \dots \dots \dots (18)$$

$$\text{for steam } k_s = \frac{-1}{\rho_s} \left( \frac{\partial \rho_s}{\partial P} \right)_{T_g} \dots \dots \dots (19)$$

$$\text{for non-condensable gases } k_n = \frac{-1}{\rho_n} \left( \frac{\partial \rho_n}{\partial P} \right)_{T_g} = \frac{1}{P_n} \dots \dots \dots (20)$$

$$\text{for gaseous phase } k_g = \frac{-1}{\rho_g} \left( \frac{\partial \rho_g}{\partial P} \right)_{T_g} = \frac{-1}{\rho_g} [\rho_s k_s + \rho_n k_n] \dots \dots \dots (21)$$

## 2.2 Assumptions

For investigation, a UTEPUV (Uneven Temperature Equal Pressure and Unequal Velocity) model is used, which has equal phase pressure (system pressure) but unequal phase velocities and temperatures. In addition, the steady flow region has been chosen [21-23]

The following are the essential assumptions for approximation of a model's problem description:

- (1) The pressures of the two components (liquid metal and non-condensable gas) are equivalent.
- (2) On the interface, component velocities are equivalent.
- (3) There is no force between linked masses.
- (4) The area function of the through passage segment is continuous.

## 2.3 Solution methodologies

Mathematical expressions that determine fluid movement and are classified as partial differential equations in gradients of physical parameters such as temperature, vapor pressure, and mass flow rate may be solved using the technique of characteristics. The method of characteristics is an approach [1,2,3 and 7] for solving partial differential equations. It usually relates to first-order equations, although the approach of characteristics applies to any hyperbolic partial differential equation in the broad sense. A partial differential equation is reduced to a series of ordinary differential equations across whereby the solution may be interconnected from certain initial information given on an appropriate hypersurface. A one-dimensional convection-diffusion model has been constructed for the approach. The study of a system of conservative eigenvalues can reveal information about its computational orientation. The TFM structure can be categorized as well-posed or ill-posed considering the nature of the eigenvalues, as reported by many researchers. This part contains the essentials of this method for your convenience. The mathematical model (1) to (7) can be simplified to the linear example given by equation (22).

$$I(\bar{z}) \frac{\partial \bar{z}}{\partial t} + J(\bar{z}) \frac{\partial \bar{z}}{\partial x} = C(\bar{z}) \dots \dots (22)$$

Here  $\bar{z}$  is the independent primary variable, and the bar represents a 7th order column matrix of direct orthogonal physical quantities (variables) in the current issue  $[x \ e_g \ e_f \ V_g \ V_f \ \alpha_g \ P]^T$  (i.e., system state properties). The matrices 'I' and 'J' are both '14 x 14' square matrices. 'C' is an n-dimensional vector with only algebraic terms in it. Formulation (22) creates a system of first-order linear mathematical models for 7-unknowns with two independent variables that are quasi-linear (x and t). Cramer's formula can be used to represent the variations. In our example, the characteristics  $c^*$  are derived from the approximate solution below (23).

$$|I - (1/c^*)J| = 0 \dots \dots (23)$$

The kind of instability of the model is determined by the nature of the features derived from the preceding equation [14]. Equations are no longer hyperbolic when the eigenvalues are complex integers. The goal was to determine the size of the domain in which the model's hyperbolic character may be found. The matrices I and J for the basic fluid thermo-dynamic flow equations were derived from the above-mentioned study of seven numerically suitable equations (1) to (7).

## 2.4 Getting Eigenvalues

Because finding a mathematical formulation for  $c^*$  is challenging, the estimates of  $c^*$  for various values are calculated with numerical methods. To get the full view, the characteristics of the given equation were determined for multiple samples of pressure, void fractions (sum of volume fraction of vapor plus gas fields), and  $V_g/V_f$  (slip ratio). Under the postulated accident scenarios that generate two-phase, multi-component flow, the roots of the characteristics of a thermal-hydraulic analytic model of a European WCLL test blanket system design are found (lead-lithium, steam, and non-condensable gases mixture).

To cover the whole two-phase functioning range, the chosen void fraction range is  $1 \times 10^{-5}$  to 0.999 with a minimum increment of 0.0001. The specified slip ratio range is 0 to 100 with an acceptable increment of 0.05 to incorporate all the pictures of fluid flow patterns for various phasic velocity samples. The instance of a negative slip ratio for which the two fluids are flowing in the opposite directions is not shown here (in the absence of force flow) since these sample fluid conditions show the same characteristics. From equation (23), we can easily find out the complete set of eigen roots [7]. The equation (23) yields a seventh-order algebraic equation, which has been calculated to provide estimates of the eigen roots  $c^*$  for various matrix elements of the matrices I and J given in figures 1 and 2 (i.e., for different sample fluid pressure, void percent, gas mass fractions, and phase flow velocities). The sample values of void fraction and slip ratio have been changed for a given significance level of system pressure and liquid phase velocity. The areas in which the Eigen roots appeared complex were determined. The system geometrical and physical parameters for the values of analytical model characteristics are taken from the literature. The fluid properties like specific enthalpy and specific fluid phasic densities for the different components in the flow at various system pressures were acquired using standard thermodynamic tables and correlations from the literature [24-28].

$$\text{Matrix I} = \begin{bmatrix} \alpha_g X_n \left( \frac{\partial \rho_g}{\partial X_n} \right) + \alpha_g \rho_g & \rho_g X_n & 0 & 0 & \alpha_g X_n \left( \frac{\partial \rho_g}{\partial e_g} \right) & 0 & \alpha_g X_n \left( \frac{\partial \rho_g}{\partial P} \right) \\ \alpha_g \left( \frac{\partial \rho_g}{\partial X_n} \right) & \rho_g & 0 & 0 & \alpha_g \frac{\partial \rho_g}{\partial e_g} & \alpha_f \frac{\partial \rho_f}{\partial e_f} & \alpha_g \frac{\partial \rho_g}{\partial P} + \alpha_f \frac{\partial \rho_f}{\partial P} \\ \alpha_g \left( \frac{\partial \rho_g}{\partial X_n} \right) & \rho_f & 0 & 0 & \alpha_g \frac{\partial \rho_g}{\partial e_g} & -\alpha_f \frac{\partial \rho_f}{\partial e_f} & \alpha_g \frac{\partial \rho_g}{\partial P} - \alpha_f \frac{\partial \rho_f}{\partial P} \\ 0 & 0 & \alpha_g \rho_g & \alpha_f \rho_f & 0 & 0 & 0 \\ 0 & 0 & 1 + \frac{C \rho_m^2}{\rho_g \rho_f} & -1 - \frac{C \rho_m^2}{\rho_g \rho_f} & 0 & 0 & 0 \\ \alpha_g e_g \left( \frac{\partial \rho_g}{\partial X_n} \right) & \rho_g e_g + P & 0 & 0 & \alpha_g \rho_g + \alpha_g e_g \frac{\partial \rho_g}{\partial e_g} & 0 & \alpha_g e_g \frac{\partial \rho_g}{\partial P} \\ 0 & -\rho_f e_f - P & 0 & 0 & 0 & \alpha_f \rho_f + \alpha_f e_f \frac{\partial \rho_f}{\partial e_f} & \alpha_f e_f \frac{\partial \rho_f}{\partial P} \end{bmatrix}$$

Fig.1. Elements of matrix I

$$\text{Matrix J} = \begin{bmatrix}
 \alpha_g V_g X_n \left( \frac{\partial \rho_g}{\partial X_n} \right) + \alpha_g \rho_g V_g & \rho_g V_g X_n & \alpha_g \rho_g X_n & 0 & \alpha_g V_g X_n \left( \frac{\partial \rho_g}{\partial e_g} \right) & 0 & \alpha_g V_g X_n \left( \frac{\partial \rho_g}{\partial P} \right) \\
 \alpha_g V_g \left( \frac{\partial \rho_g}{\partial X_n} \right) & \rho_g V_g - \rho_f V_f & \alpha_g \rho_g & \alpha_f \rho_f & \alpha_g V_g \frac{\partial \rho_g}{\partial e_g} & \alpha_f V_f \frac{\partial \rho_f}{\partial e_f} & \alpha_g V_g \frac{\partial \rho_g}{\partial P} + \alpha_f V_f \frac{\partial \rho_f}{\partial P} \\
 \alpha_g V_g \left( \frac{\partial \rho_g}{\partial X_n} \right) & \rho_g V_g + \rho_f V_f & \alpha_g \rho_g & -\alpha_f \rho_f & \alpha_g V_g \frac{\partial \rho_g}{\partial e_g} & -\alpha_f V_f \frac{\partial \rho_f}{\partial e_f} & \alpha_g V_g \frac{\partial \rho_g}{\partial P} - \alpha_f V_f \frac{\partial \rho_f}{\partial P} \\
 0 & 0 & \alpha_g \rho_g V_g & \alpha_f \rho_f V_f & 0 & 0 & 1 \\
 0 & 0 & V_g & -V_f & 0 & 0 & \left( \frac{1}{\rho_g} - \frac{1}{\rho_f} \right) \\
 \alpha_g V_g e_g \left( \frac{\partial \rho_g}{\partial X_n} \right) & \rho_g e_g V_g + P V_g & \alpha_g \rho_g e_g + \alpha_g P & 0 & \alpha_g \rho_g V_g + \alpha_g e_g V_g \frac{\partial \rho_g}{\partial e_g} & 0 & \alpha_g e_g V_g \frac{\partial \rho_g}{\partial P} \\
 0 & -\rho_f e_f V_f - P V_f & 0 & \alpha_f \rho_f e_f + \alpha_f P & 0 & \alpha_f \rho_f V_f + \alpha_f e_f V_f \frac{\partial \rho_f}{\partial e_f} & \alpha_f e_f V_f \frac{\partial \rho_f}{\partial P}
 \end{bmatrix}$$

Fig.2. Elements of matrix J

## 2.5 Virtual Mass Force and diffusion forces in liquid metal and gases multi-component two phase flow

In two-phase flows, a bubble carries some liquid mass as it passes through a quiescent liquid. This portion of the liquid mass should acquire bubble velocity, causing a virtual increase in bubble mass. This can happen in various physical situations, such as when a particle or droplet travels through a gaseous environment. In this situation, the particle's gas mass is negligible compared to the particle's mass; hence the momentum balances are unaffected. As a result, simulated mass is often ignored when solid particles or liquid droplets migrate in a gaseous atmosphere. The size of this force is governed by the density relationships between the phases in the case of two fluids flowing together. There is no considerable differential acceleration between phases when driving factors such as external force from the pump and gravity forces influence all phases equally, and the densities of both phases are equivalent. Hence virtual mass effects are weak and may be ignored. Virtual mass forces are required in liquid metal, vapor, and non-condensable two-phase flow because the scattered gaseous phase has a substantially lower density than the continuous phase. Many studies have suggested that virtual mass concepts be used in multi-phase simulations to improve the well-posedness and numerical stability of the TFM model's discretized system of equations. Still, it has been claimed that it has no effect on simulation accuracy in predicting two-phase flow phenomena (Drew et al. [18], Geurst et al. [19], Watanabe & Kukita [20]). This is true for a wide range of bubbly flows encountered in industrial settings, such as flows in huge channels in nuclear reactors, where acceleration effects are minimal. The pressure gradient equations for bubbly flows in a nozzle with a high contraction ratio exhibit considerable differences when virtual mass force is utilized in the modeling. Therefore, the virtual mass force should be addressed in every situation to improve numerical stability and model predictability of physical two-phase flow processes. The Virtual Mass Effects for vapor bubble acceleration formulation in the SIMMER code is considered from the RELAP5 code developed model.

Whenever the bubble expands through a liquid, it absorbs part of the liquid underneath it. The acceleration of the surrounding fluid causes a virtual mass force. Because it virtually boosts the mass of the bubble, it is referred to as virtual mass force. Drew et al. [18] investigated the influence of virtual mass force on the physics and stability of the two-fluid model (TFM).

The virtual mass force formulation is provided by formula (24) and may be found in the literature [19]. The virtual mass force in RELAP5 is optimized by ignoring the spatial derivatives. Factual errors in estimating the spatial derivative component of the term for the relatively coarse nodalizations employed in system representations, according to the handbook (Information Systems Laboratories 2003).

$$F_{vm} = \alpha_g(1 - \alpha_g)\rho_m C \left\{ \frac{\partial V_g}{\partial t} - \frac{\partial V_f}{\partial t} + V_g \frac{\partial V_g}{\partial x} - V_g \frac{\partial V_f}{\partial x} \right\} \dots \dots (24)$$

Here  $F_{vm}$  is the virtual mass force and C is the virtual mass coefficient.

Since the value of virtual mass coefficient C is highly dependent on the flow regime, bubble geometry and bubble size under the two-phase flow conditions. As of the current state of the art, the flow regimes of the liquid metal are not well-developed hence specific values of virtual mass coefficient are not available. Therefore, in the current investigation the value of C is taken between 0 to 1. An optimized value of 0.5 is considered as a sample value based on air water two phase flow [21].

In the case of a two-phase flow, it is well acknowledged that the diffusion force caused by the concentration gradient of the dispersion medium acts on the fluid. This force addition in the momentum equation is critical for two-phase flows involving liquid-metal and gas since it can significantly impact the modeling of such flows and affect the mathematical characteristics, which has been analyzed in this paper employing eigenvalue and linear stability analysis. Since the absence of diffusion force coefficients, a wide range of coefficient values is taken to know the effect on the characteristics of the proposed TFM.

## 2.6 Sample fluid conditions of water-cool WCLL European Test Blanket System

It has been demonstrated in various previous literature that the TFM characteristics are highly dependent on the sample fluid flow conditions. Therefore, to investigate the characteristics of the TFM for gas-liquid metal two-component two-phase flow, one of the most suitable systems to incorporate the physical properties in the model is the water-cooled Test Blanket System. The European WCLL blanket is made of reduced activation ferritic-martensitic steel (Eurofer) as the structural material. Liquid Lithium-Lead (PbLi) eutectic with 90 % Pb and 10 % Li 6 as the breeder, neutron multiplier, and tritium carrier. Water used as coolant like pressurized water reactor (PWR) like fluid conditions (295-328°C, 15.5 MPa). The two-fluids water Lead-Lithium and non-condensable gases can come in contact in a leak accident, resulting in a two-component, two-phase gas-vapor and liquid metal flow. This incident is one of the probable events that can occur during the operational life of TBS and is discussed in detail in the literature [32-35]. The system's geometric values and physical parameters (utilized in the current analysis) can be found in the literature [32]. A brief information about the WCLL TBM geometry is discussed in this section for the convenience of the readers. In the thermal design of the WCLL TBS, the heat load on WCLL is considered as the average surface heat flux on the FW (0.3 MW/m<sup>2</sup>) and nuclear heat deposition on each component in the TBM module.

The FW is made of Eurofer and thickness 25 mm; a 2 mm thick tungsten layer covers the plasma-facing region. As indicated in the diagram, the water coolant runs in a countercurrent direction via square channels measuring 70.7 mm by 13.5 mm with a pitch of 13.5 mm (Fig. 3). To guarantee the symmetry of the breeding units, the location of FWs channels is symmetrical concerning the plane of TR and plates. There are ten cooling channels in each breeding unit. Water enters at 295°C and leaves at a temperature of 328°C, with a pressure of 15.5 MPa. Figure 3 shows the schematic of the WCLL-TBS, whose geometrical and operational system parameters are utilized in the study presented. Under the accident condition, the high-pressure water and Lead-lithium can leak into the VV. Therefore, the mass continuity equation for both gas and liquid metal must incorporate the change in the mass flow of each component in the breached system. Two separate momentum equations are also needed to include each fluid component's velocity variation in the breached system. Since both fluids have different enthalpy (when separated) and the heat load is continuously added to the channel wall. Two separate energy conservation equations should be defined for the two fluids to determine the energy exchange between fluid and part of energy transported by each fluid. The complete set of equations is defined in section (1.2). The evaluation of this TFM and its characteristics under varying sample fluid conditions and fixed geometrical conditions are discussed in the next section.

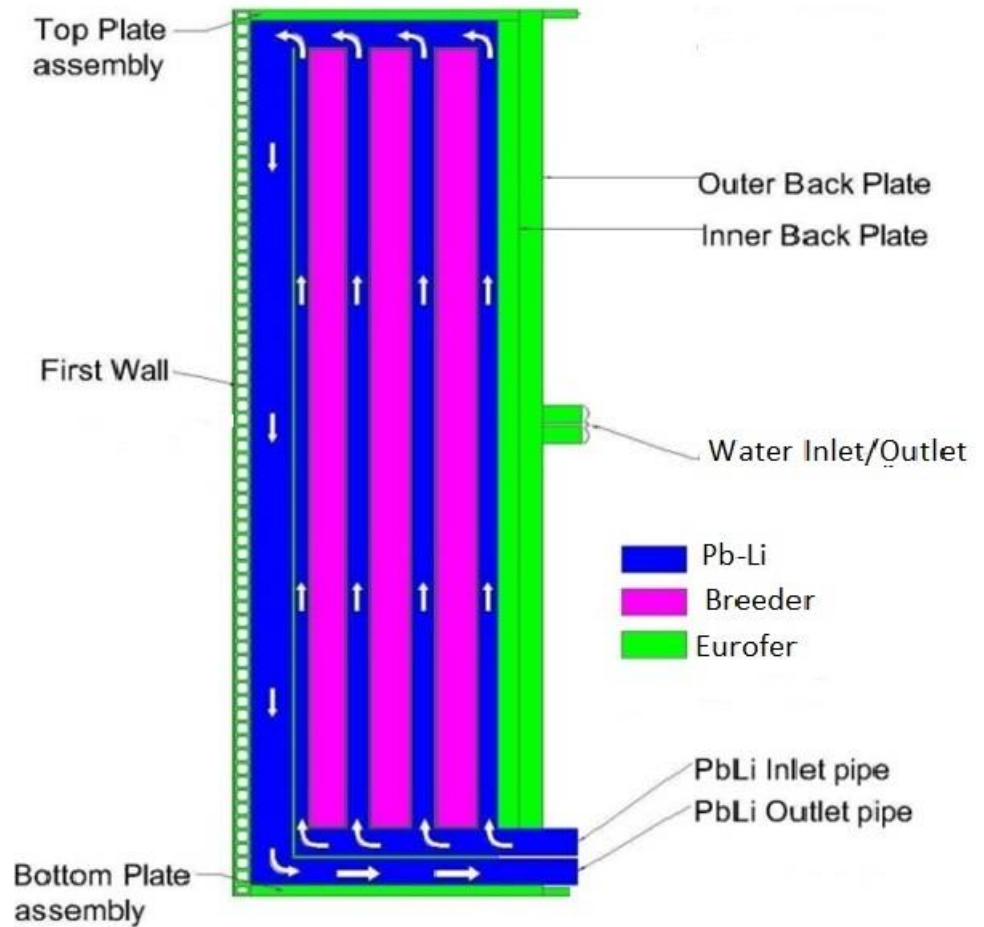


Fig. 3 Schematic of Water-Cooled Lithium-Lead (WCLL) Test Blanket System (TBS)

### 3 Results and analysis

#### 3.1 Region of well-posed/ill-posedness

We initially discovered virtually all flow patterns (sample dynamic fluid conditions) of the system dynamic conditions (area of complex features) throughout this section, in which the TFM eigenvalues for two-component and two-phase liquid-metal-gas flow turn complex. TFM becomes non-hyperbolic or ill-posed in specific reference fluid circumstances systems. The fluid reference parameters for the system geometry described in Figure 3 were achieved. The study includes all potential fluid conditions of light water reactors (LWRs) for transient and accident situations. The present part focuses only on determining the non-hyperbolic (complex features) area. From 0 to 1, the empty fraction is increased. It uses a 0.0001 increment to cover all conceivable two-phase fluid conditions that might occur during the accident scenario in the TBM shown in figure 3. The slip ratio is tuned to cover the whole range of liquid and gas phasic velocities of interest. The following part discusses the physical effects of the position and amplitude of the system's complex roots on the solution of non-hyperbolic systems. The study of linear stability is also discussed in the next section. Here on error rates of growth, we looked at the impact of different forces in the momentum equations, system parameters, and closure/constitutional connections. According to the study, only two of the system's six eigenvalues are complex (corresponding to the phasic momentum equations) for flow regimes, while the other four are always real. It indicates that good force modeling in the momentum equation is extremely desired for more correctly simulating two-phase flow phenomena without sacrificing vital physical information. Furthermore, to prevent the systems modeling instability that arises from the system model's ill-posed character due to the governing equations' secondary physical forces consideration.

Our major goal in this research is to look at the well-posed/ill-posed nature of a system code called TFM, which can simulate the thermal-hydraulic properties of liquid metal/non-condensable gases/steam multi-component two-phase flow for all fluid flow conditions. The TFM has initially been developed and thoroughly validated against experimental findings for the RELAP and TRACG light-water nuclear reactor thermal-hydraulic codes and has since been extensively applied by several other recently developed system codes such as MELCOR, SIMMER and others to investigate the thermal-hydraulic characteristics of advanced reactors. Since then, it has been extensively demonstrated that the basic TFMs are ill-posed for certain fluid flow regimes, particularly at the greater void percentage and phasic velocity difference values. As a result, practically all system codes use some method to regularize their model to diminish the ill-posedness area in fluid flow regimes. The RELAP5 code model improves the well-posedness of the governing set of equations for fluid (water) flow regimes by using the virtual mass force part of the momentum equations. The proper addition of virtual mass force (which is highly dependent on fluid flow regimes) may greatly enhance the model's well-posedness, but it cannot make the model unconditionally well-posed. The flow regimes and flow regime-dependent constitutional/closure relationships for liquid-metal-non-condensable multi-component-two-phase flows are not well-developed, and only limited data without validation is available. So, under such constrained settings, we employed a wide variety of virtual mass value coefficients to investigate the influence of virtual mass force variation on the features of liquid-metal-non-condensable multi-component-two-phase flows. Figure 4 depicts the region of complex characteristics for various values of the coefficient of virtual mass ( $C$ ) for system conditions ( $P=8$  MPa,  $V_f=1$  m/s,  $V_g$  varies one m/s to 50 m/s, and void fraction 0 to 1), where "\*" denotes the complex characteristics region, in which two of the six roots are complex in nature, but "r" denotes the entire real characteristics region. Figure 4 shows that increasing the virtual mass coefficient reduces but does not eliminate the area of ill-posedness in the system of equations. An appropriate flow regime-dependent virtual mass coefficient is required to determine the precise border of the zone of complex features. The variation, on the other hand, would reflect the results in figure 4. This demonstrates that the considered TFM (for light water) and flow regimes and constitutional/closure relationships for liquid-metal -non-condensable multi-component-two-phase flows can be used for simulation of liquid-metal non-condensable multi-component-two-phase flows by avoiding some sample fluid flow conditions. Either through a change in system geometric design or through additional safety arrangements that can eliminate the probability of system failure. Although this is impractical and unaccepted by regulatory agencies, various regularization strategies based on missing physics to the momentum equations that lessen the system's ill-posedness are explored in the following sections.

For the system's parameters stated in figure 3, figure 5 is plotted to identify the area of complicated features for extremely high values of slip ratios.

### 3.2 An examination of the features roots (Eigen spectrum)

The character of roots is determined by plotting the attributes of Eigen roots on the complex plane. In this subsection, real and imaginary eigenvalues are addressed concerning the solution of an equation system. We have a seventh-order characteristics equation using as an example for the two-component, two-phase flow of liquid metal and non-condensable gases (7 eigenvalues). In the last 50 years, the basic mathematics that connects the Eigenvalues of the mathematical model (hyperbolic and elliptic) to the error in the computational domain has advanced significantly, and some of the most recent and reasonable implementations that introduce this mathematics are [1-6]. This mathematics affirms that:

1. if the mathematical model of the system has complex roots, it is non-hyperbolic as well as ill-posed, and thus analysis techniques very often generate inconsistent findings,
2. the error in processing parameters is modified together with input data, causing error progression in the time of the order, and thus the obtained result from it would be incredibly susceptible to any deviation (even relatively insignificant) in the input variables,
3. any perturbation in the system produces conflicting results, and
4. Any perturbation in the It is also apparent that a bit of rising in the imaginary component of complex roots boosts the system's susceptibility (more susceptible to errors).

The Eigenvalue spectra in the complex plane for various virtual mass coefficient  $C$  values are described in Figure 6.  $P=15.5$  MPa,  $V_g$  increases from 0.001 to 5 m/s,  $V_f=0.001$  m/s,  $g=0$  to 1, and  $C$  fluctuates from 0.0 to 1.0 is the other system sample circumstances used as input values, which correspond to the real location of eigenvalues in the complex plane. The eigenvalue spectrum in the complex plane is a parametric variation (slip ratio and void %) of TFM's six basic eigenvalues. Figure 6 shows that increasing the virtual mass coefficient increases the imaginary and real parts of the complex roots, directly proportional to the error growth rate in the solution [1 and 2] and hence increases the solution domain instability. Figure 6 illustrates the necessity of knowing the correct value of the virtual mass coefficient in two-phase flow simulations of liquids, metals, and gases.

It is also worth noting that all distinctive roots remain realistic for a slip ratio of less than 3. When the slip ratio surpasses 3, the roots of the characteristic may become complex. It has been observed that only two of the six characteristic roots ( $C_7^*$ ,  $C_8^*$ ,  $C_9^*$ ,  $C_{10}^*$ ,  $C_{11}^*$  and  $C_{12}^*$ ) become complex under certain thermal-hydraulic situations, while the other eight roots ( $C_1^*$ ,  $C_2^*$ ,  $C_3^*$ ,  $C_4^*$ ,  $C_5^*$ ,  $C_6^*$ ,  $C_{13}^*$  and  $C_{14}^*$ ) remain genuine. We find that when the slip ratio rises, the imaginary component of eigenvalues rises as well. Many prior works of literature for light water and two-phase airflow make the same finding.

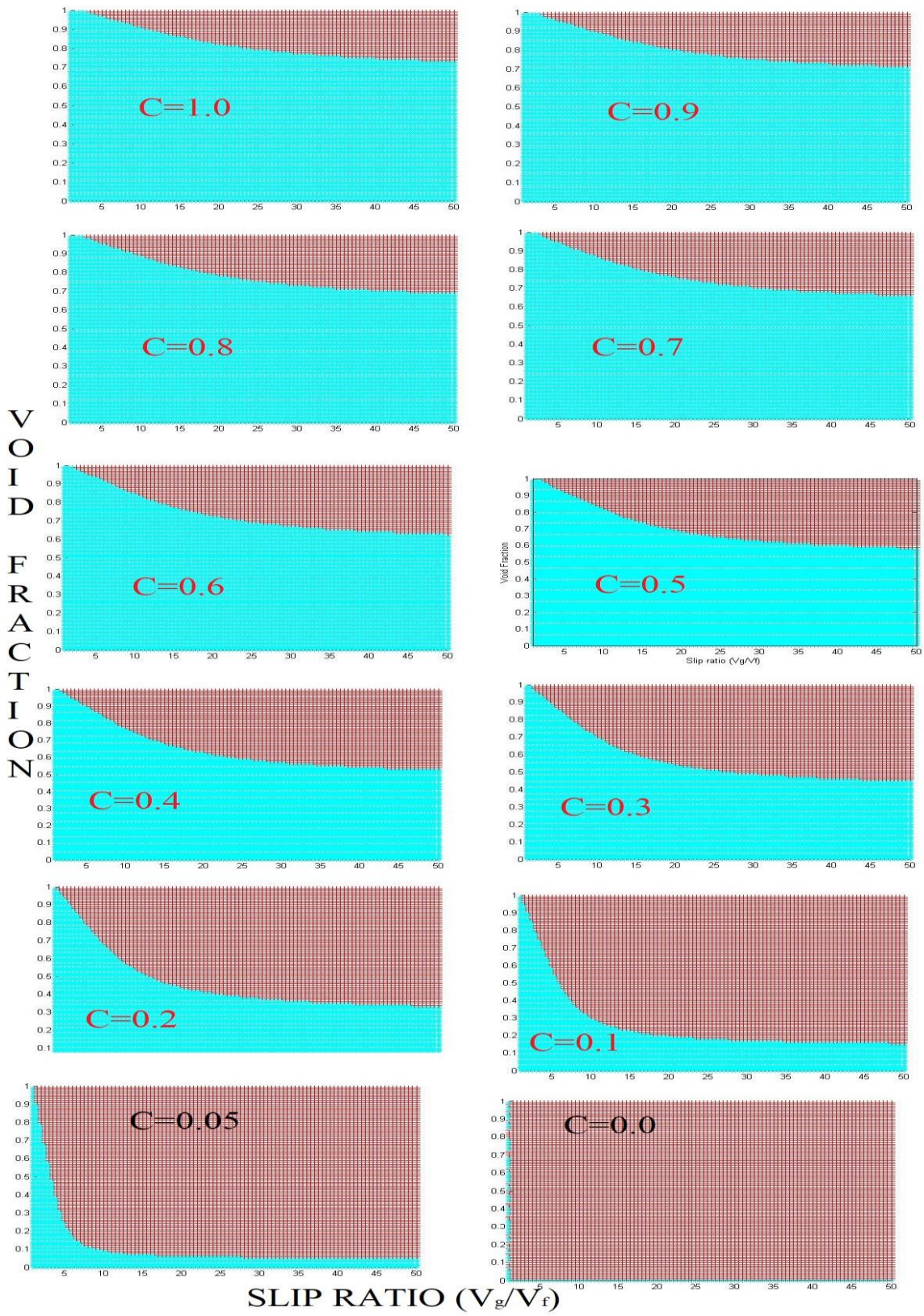


Fig. 4 Complex Characteristics area for different values of Coefficient of virtual mass (C) for system conditions ( $P=15.5$  MPa,  $V_f=0.001$ ,  $V_g$  varies 0.001 to 0.05 and void fraction 0 to 1 "\*" complex region "\*" real region

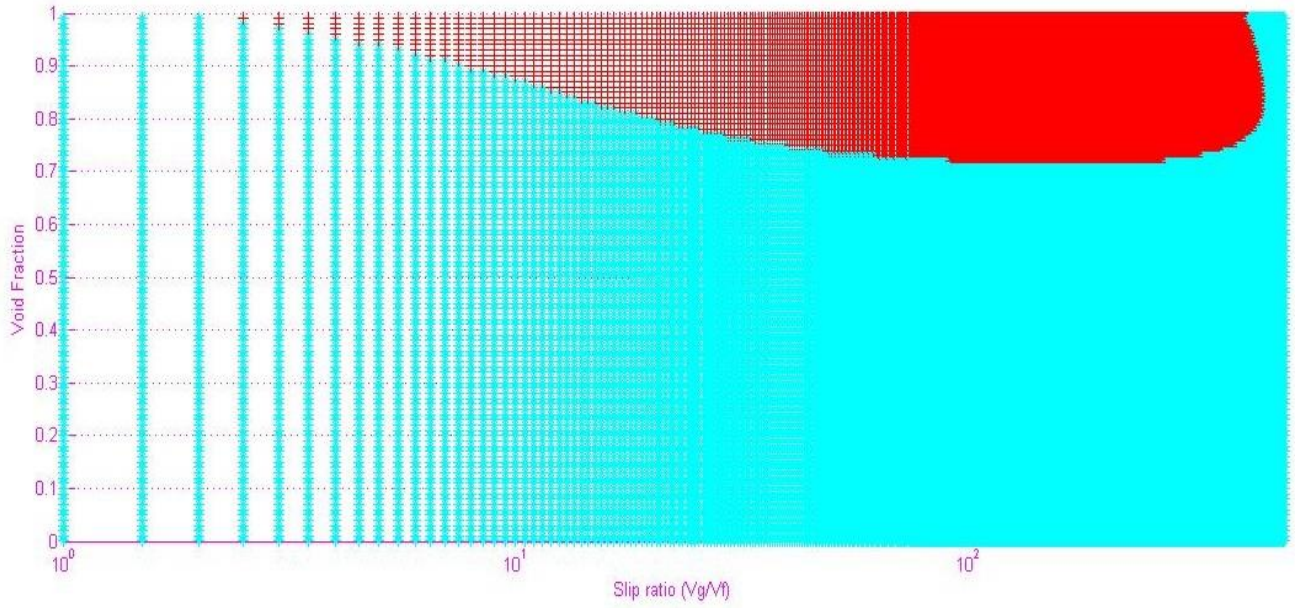


Fig. 5 Complex Characteristics area for system conditions ( $C=0.5$ ,  $P=15.5$  MPa,  $V_f=0.001$ ,  $V_g$  varies 0.001 to 1 m/s and void fraction 0 to 1) "\*" complex region "\*" real region

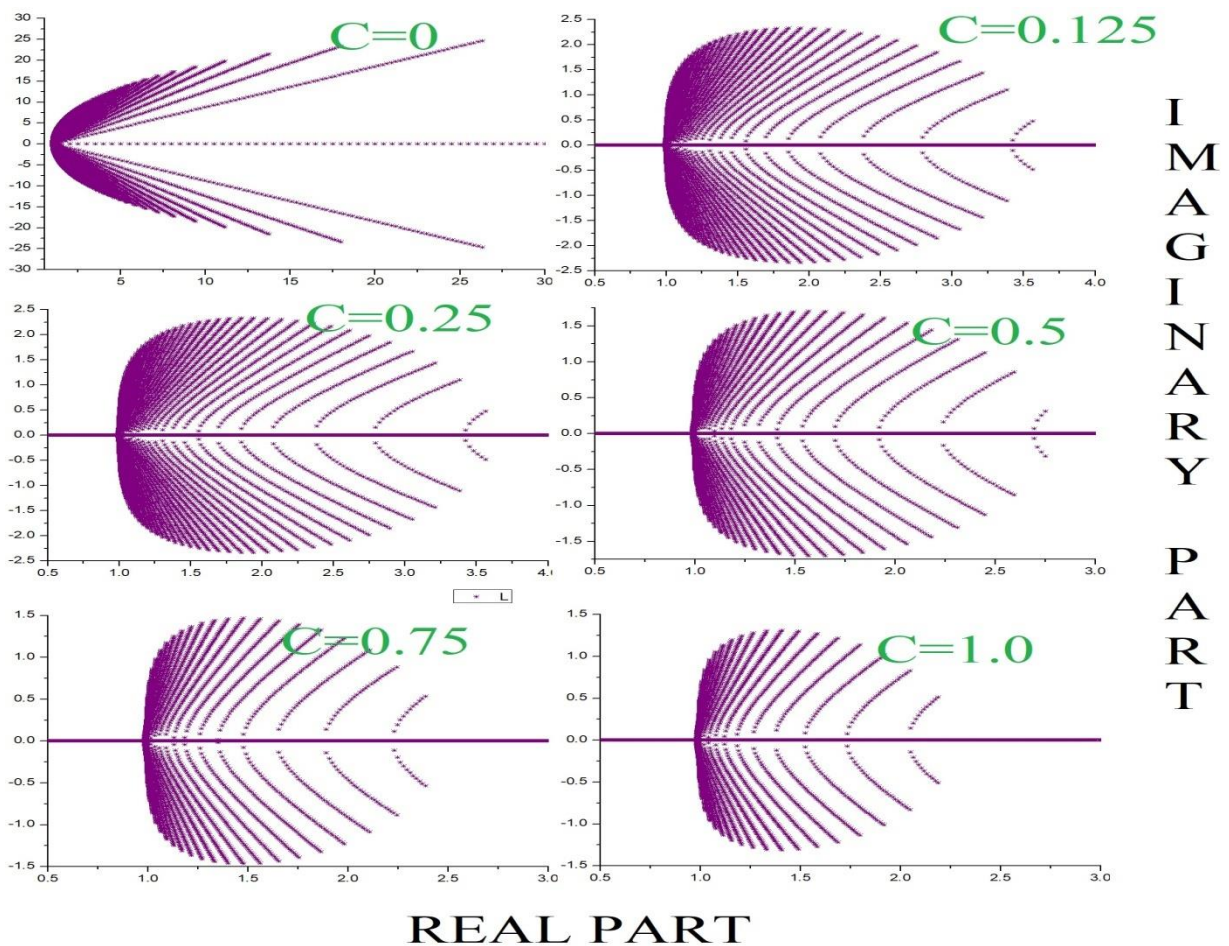


Fig. 6 Eigenvalue spectrum in complex plane for different values of virtual mass coefficient  $C$  the other system sample conditions are  $P=15.5$ ,  $V_g=1$  to 50 m/s,  $V_f=1$ ,  $\alpha_g=0$  to 1 and  $C=0.0$  to 1.0

### 3.3 Dispersion analysis (linear stability analysis) for Liquid-metal-non-condensable gases two-component, two-phase flow

The WCLL-TBS is discussed in further detail in Section 2.3 of this study. In section 3.2, the eigenvalue (characteristic) analysis and its impact on system behavior are discussed. The eigenvalue findings show how well a mathematical model performs in the limit as the wavelength gets closer to zero. Perturbation assessment also referred to as dispersion analysis, has been used to describe the dynamic behavior of the system's broad wavelength range. We will look at how well the response operates at different wavelengths throughout this subsection.

We explored the linear stability of the Liquid-metal gas two-phase flow, generally known as dispersion assessment, for numerous test dynamic fluid conditions of the liquid metal and gas in this portion of the text. This segment also examines the impact of adding physical forces such as diffusion terms in the basic TFM for a two-component two-phase flow. Linear stability mathematics is well-developed, and it has lately been applied to TFM in several research [1 and 2].

Figures 7–9 show the dispersion analysis growth trend for the WCLL TBS system during transient liquid-metal breach into air channels settings using the basic SIMMER-III model and a model either with or without diffusion terms, respectively. The sample fluid conditions in this example are ( $P= 15.5$  MPa, slip ratio = 10, void percent 0.8, with various phasic velocities and diffusion coefficients). Figure 7 (a) shows the sample fluid environments wherein the system is ill-posed. After acquiring sample fluid conditions, identified parameters (void fraction=0.8 and slip ratio = 5) is used as the input parameters for the dispersion assessment that can be seen in figures 7 (b) and 7 (c) for TFM without diffusion term in momentum equations and TFM with diffusion term in momentum equations, respectively.

The fundamental TFM of SIMMER-III for Liquid-metal-gas two-phase flow is ill-posed for the given sample two-phase flow fluid circumstances since the error growth rates are high even for higher values of wavelengths, as shown in figures 7 to 9. Figures 7–9 provide a comparison of growth-rate variations with wavelength for the TFM with and without diffusion terms, as well as various slip ratio values. Figures 7 to 10 depict the influence of diffusion terms in momentum equations on growth rates. Figure 7 shows that when the basic SIMMER-III TFM does not include a diffusion component, the growth rate grows exponentially for decreasing wavelengths; therefore, the model is ill-posed in this case. Figure 7 further shows that when diffusion terms are included in SIMMER-III's basic TFM, the growth rate does not rise indefinitely and begins to decrease below a specific cutoff wavelength.

For slip ratio 20 void fraction  $g=0.8$  and system pressure =8MPa, Figure 8 illustrates the growth rates of dispersion analysis for the Basic TFM model and TFM with varied values of diffusion coefficients. Figure 9 depicts dispersion analysis growth rates for the Basic TFM model with various diffusion coefficient values for slip ratio 50 void fraction  $g=0.8$  and system pressure =15.5 MPa. By comparing figures 8 and 9, we can see that even larger diffusion coefficient values in the momentum equations cannot make the model well-posed for higher values of slip ratio, i.e., in turbulent two-phase flow of liquid metal-gas. Other TFM regularization techniques for liquid-metal and gas two-phase flow should be developed under these settings.

Figures 8 and 9 demonstrate that adding a diffusion mechanism to SIMMER-III's basic TFM eliminates disturbance's low wavelength (high frequency) harmonics. The magnitude of high wavelength (low frequency) harmonics of disturbance is unaffected by the diffusion process. As a result, adding diffusion factors to the momentum equations of SIMMER-III's basic TFM acts as a low pass filter (eliminating the high-frequency harmonics).

Figure 9 indicates that the system with diffusion terms is still ill-posed and includes low frequency fluctuations for the sample fluid condition ( $P= 15.5$  MPa, slip ratio = 50,  $V_f= 1$  m/s,  $V_g=50$  m/s, void fraction 0.8). Figure 10 demonstrates the dispersion assessment rates of growth for the basic TFM model with various slip ratios. Figure 10 shows that when the slip ratio increases, the error growth rates rise as well. That is, when the gas to liquid metal velocity is greater than a particular cutoff value (depending

on the operating characteristics), the TFM produces an ill-posed problem with wavelength-sensitive errors in the responses, and a larger slip ratio corresponds to a bigger inaccuracy in the solution space. Figure 11 depicts TFM growth rates for different slip ratios as well as TFM with diffusion coefficients of  $\vartheta_g=0.1978*10(-6)$  and  $\vartheta_f=0.127*10(-4)$  in momentum equations. When comparing figures 10 and 11, the diffusion coefficient may minimize error increase rates in lower wavelength areas. For the purposes of the analysis, the genuine value of diffusion coefficients is used. Figures 12 and 13 demonstrate the growth rates of dispersion analysis with and without diffusion terms for various void % and TFM values. Figures 12 and 13 show that a larger void fraction results in higher error growth rates in the solution domain when the gas fraction is greater than the liquid metal in complete samples for flow regimes and the gas to liquid-metal velocity ratio is significant.

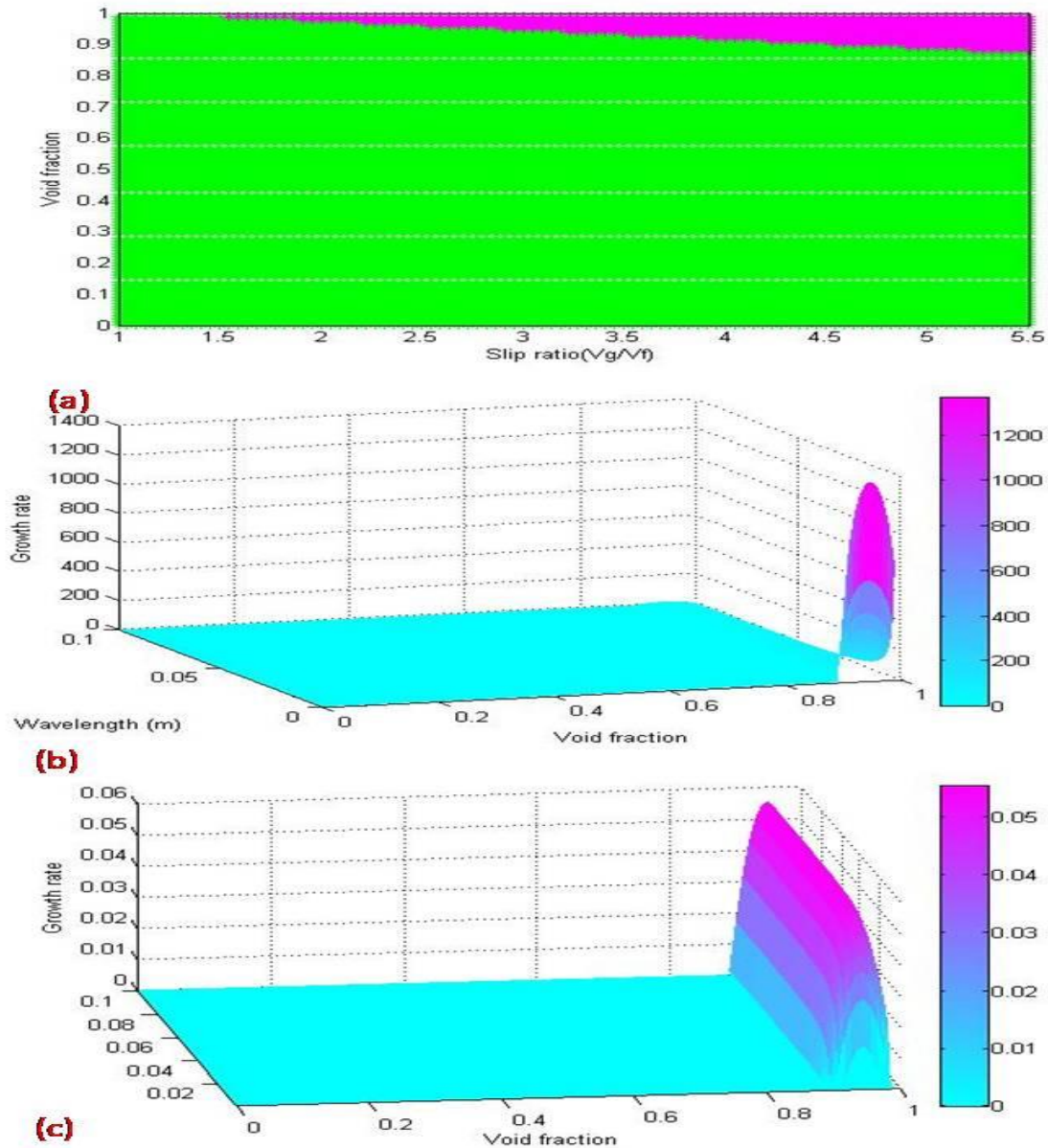


Fig. 7 (a) Complex Characteristics area for system conditions ( $P=15.5$  MPa,  $V_f=1$ ,  $V_g$  varies 1 to 5.5 and void fraction 0 to 1) "\*" complex region "\*" real region, (b) Error growth rate variation with wavelength (linear stability analysis) for basic TFM without diffusion terms in momentum equation, (c) Error growth rate variation with wavelength (linear stability analysis) for basic TFM with diffusion coefficient terms in momentum equation (viscosity=0.00001)

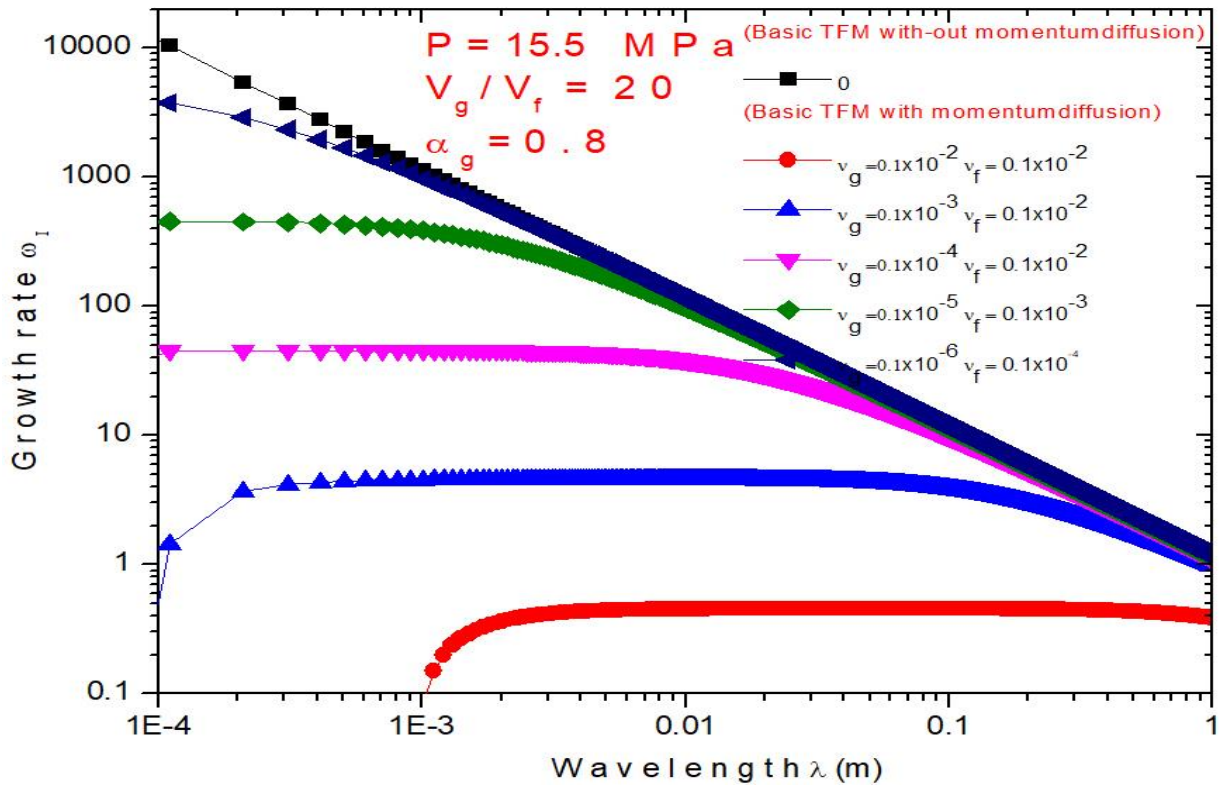


Fig. 8 Linear stability study error propagation rates for Basic TFM model and TFM with different values of diffusion coefficients for slip ratio 20 void fraction  $\alpha_g = 0.8$  and system pressure = 15.5 MPa

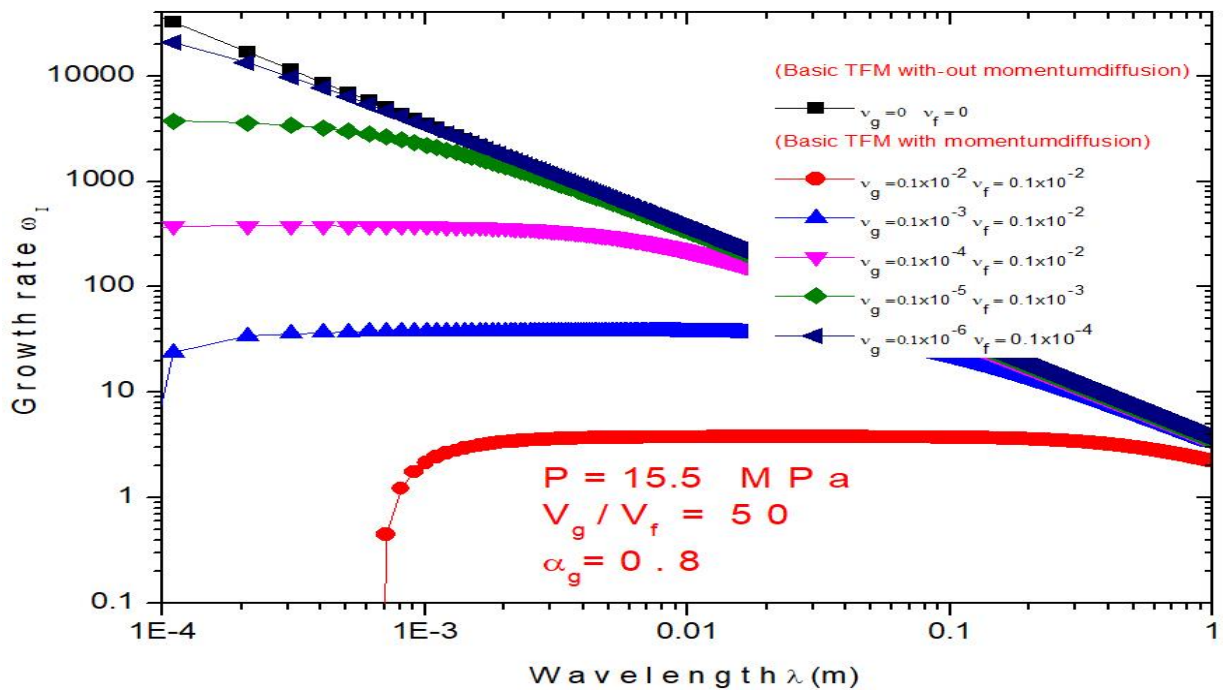


Fig. 9 Linear stability study error propagation rates for Basic TFM model and TFM with different values of diffusion coefficients for slip ratio 50 void fraction  $\alpha_g = 0.8$  and system pressure = 15.5 MPa

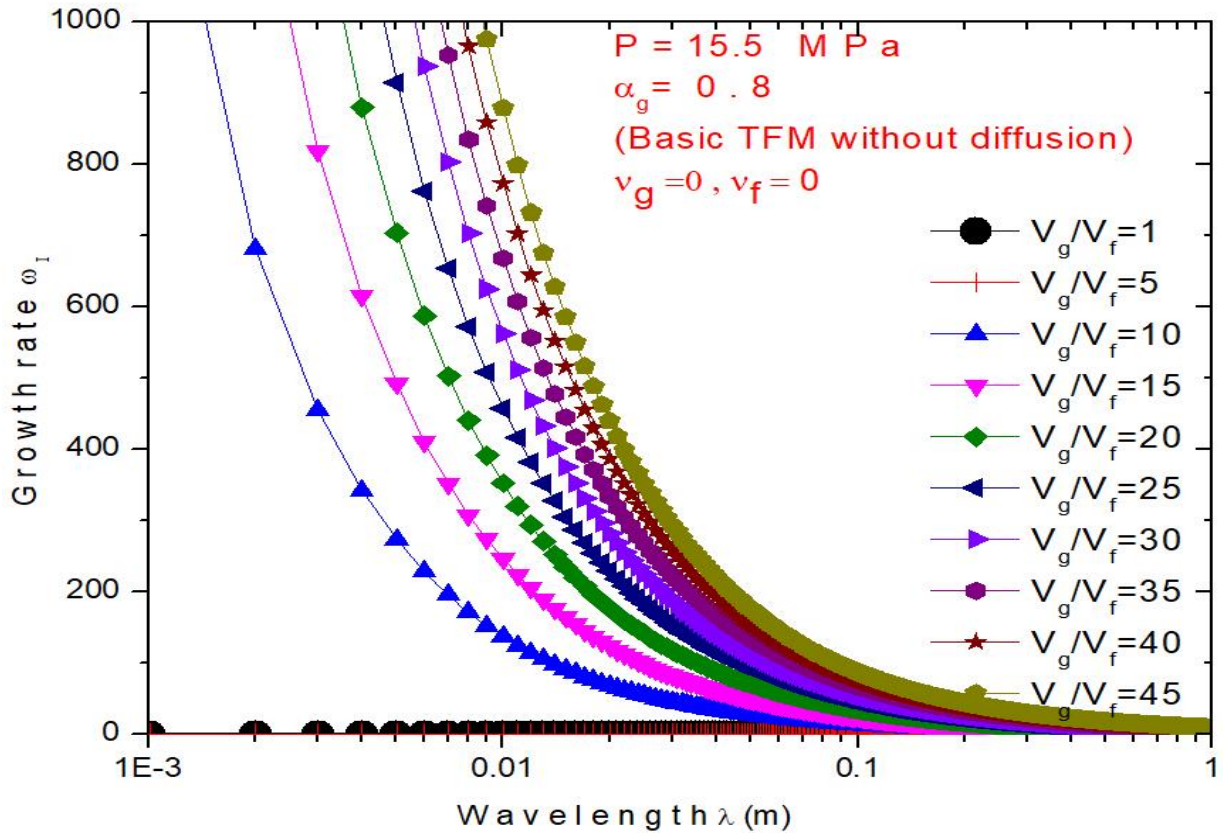


Fig. 10 Linear stability study error propagation rates for Basic TFM model with different values of slip ratios.

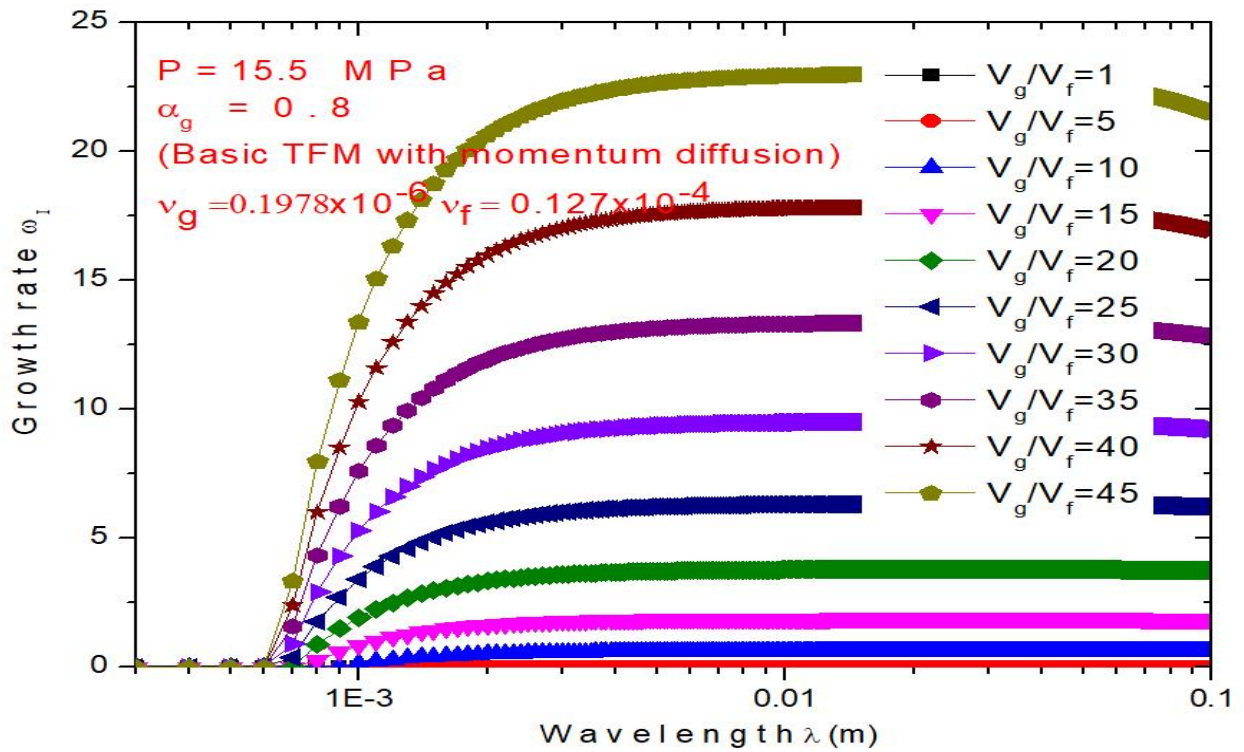


Fig. 11 Linear stability study error propagation rates for different values of slip ratios and TFM with values of diffusion coefficient  $\vartheta_g = 0.1978 \times 10^{-6} \wedge \vartheta_f = 0.127 \times 10^{-4}$ .

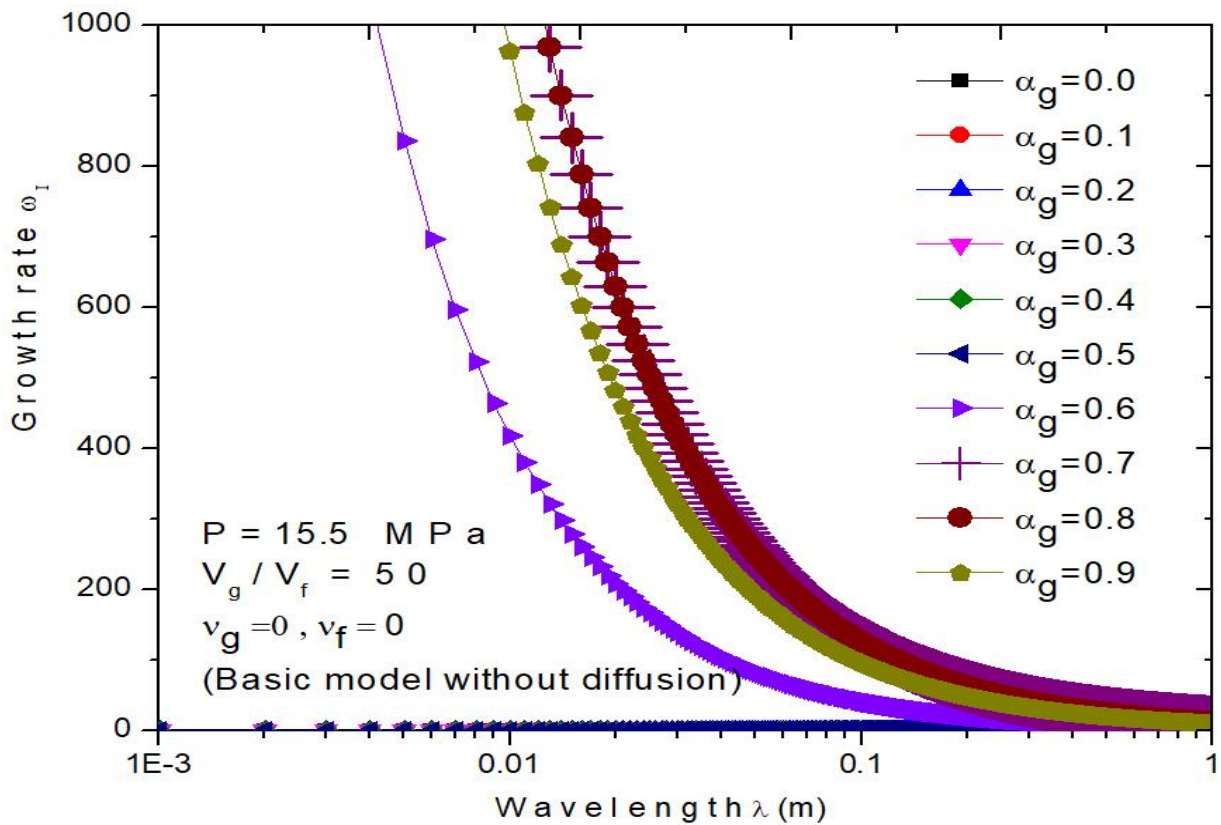


Fig. 12 Linear stability study error propagation rates for various void percentages and TFM values without diffusion coefficient values

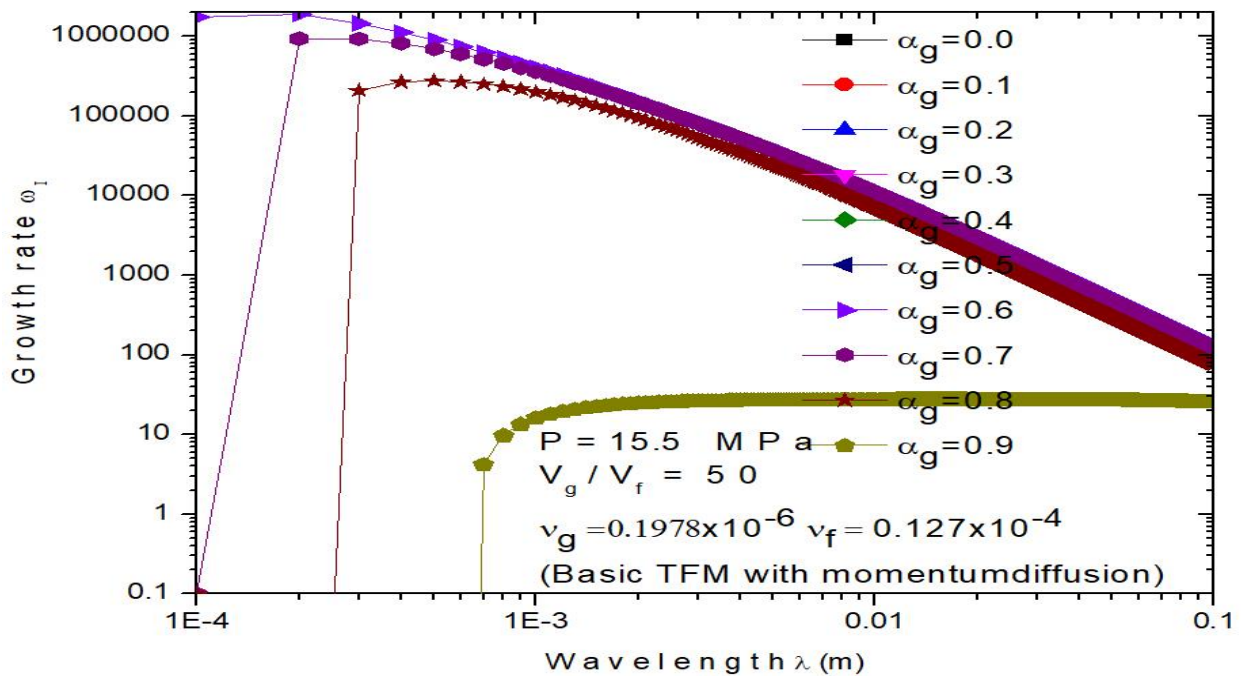


Fig. 13 Linear stability study error propagation rates for various void percentages and TFM values with diffusion coefficient values  $v_g = 0.1978 \times 10^{-6} \wedge v_f = 0.127 \times 10^{-4}$ .

## 5. SUMMARY AND CONCLUSIONS

The following are the key conclusions drawn from the research conducted for this publication.:

1. For the basic TFM to simulate multi-component and two-phase (liquid-metal and steam and non-condensable gases) flows, we estimated the range of flow regimes and fluid conditions when the features roots became complex.
2. The investigation reveals that certain of the operating spectrum's features are complex. Although the specific ramifications of this are unknown, it does provide insight into the model's mathematical features and stability.
3. The governing equations have complex properties when the void fraction and relative velocity between the liquid metal and gas approaching a critical value, and the model becomes ill-posed. This ill-posedness implies that the conclusions of the classic two-fluid model for such conditions do not reflect the actual flow mechanics inside the channel.
4. The basic two-fluid model produces relevant results when the void fraction and relative velocity between the vapor and liquid phases are less than a crucial value. This is determined by system pressure, temperature, channel diameter, gravity, and other flow characteristics.
5. The TFM liquid-metal and non-condensable gas flows are suggested to be further developed to lower the region of complex characteristics and reduce the error growth rates in the solution domain. This research focuses on eigenvalue calculations and dispersion analysis on specific instances of characteristic polynomials of approximations of the convenient form of the governing equations.
6. As a result, these conclusions are based on minimum sample size and apply to the SIMMER-III code based two-fluid model study. The analysis shows that the results for Liquid-metal, vapor and non-condensable gases multi-component, two-phase flow are quite different (characteristics roots spectrum and error growth rate patterns) from the air and water two-component two-phase flow and highly sensitive to the virtual mass and diffusion coefficients in the momentum transfer equations. This is due to the high density of liquid metals compared to liquid water which results in strong virtual mass force in liquid-metal gas two phase flows.
7. As a result, it is strongly advised that for such flows, the virtual mass coefficient and diffusion coefficients be handled more precisely, as these coefficient values significantly impact proposed TFM prediction accuracy, and there has been very little research on how to estimate these coefficients values.

## ACKNOWLEDGEMENTS

This work has been carried out within the framework of the HORIZON2020, Call H2020-MSCA-IF-2020, funded by the European Research Executive Agency (REA) via the Marie Skłodowska-Curie Actions (Grant Agreement No 101030496). Although all the experimental facilities for the experimental campaign are made available by ENEA Brasimone Research Centre. However, the ideas and thoughts presented are solely those of the author(s) and do not necessarily represent the views or opinions of the European Union or the European Commission. They are not the responsibility of the European Union or the European Commission.

**Supplementary Materials:** N. A.

**Author Contributions:** “Conceptualization, Satya Prakash Saraswat; methodology, Satya Prakash Saraswat; software; formal analysis, Satya Prakash Saraswat.; investigation, Satya Prakash Saraswat, validation Satya Prakash Saraswat, Prakash Saraswat, resources, Satya Prakash Saraswat, data curation, N.A.; writing—original draft preparation, Satya Prakash Saraswat.; writing—review and editing, Satya Prakash Saraswat, funding acquisition, Satya Prakash Saraswat.

All authors have read and agreed to the published version of the manuscript.” (“All authors have read and agreed to the published version of the ...”)

**Funding:** “The research work has received funding from the Research Executive Agency, EUROPEAN COMMISSION, under Horizon 2020 Marie Skłodowska-Curie Individual Fellowship (H2020-MSCA-IF-2020) under grant agreement No 101030496.”

**Data Availability Statement:** N. A.

**Conflicts of Interest:** no

## Nomenclature

### English

A	Cross-sectional area
$B_x$	body force in x coordinate direction (m/s <sup>2</sup> )
$B_y$	body force in y coordinate direction (m/s <sup>2</sup> )
C	coefficient of virtual mass,
C	Column matrix of algebraic terms
$C_{img}$	Imaginary part of complex eigenvalue
$C_p$	specific heat at constant pressure (J/kg. K)
$C_v$	specific heat at constant volume (J/kg. K),
$c^*$	eigenvalue or characteristics root
$C_0$	courant limit
dy/dx	Change in Y direction (perpendicular to flow direction) with X direction
f	inter-phase friction factor
<b>f</b>	liquid phase
<b>g</b>	vapor phase
h	specific enthalpy (J/kg)
$h_f^*$	Liquid phase enthalpies associated with bulk interface mass transfer
$h_g^*$	Gaseous phase enthalpies associated with bulk interface mass transfer
$H_{ig}$	vapor interface heat transfer coefficient per unit volume
$H_{if}$	liquid interface heat transfer coefficient per unit volume
$h_{gf}$	sensible (direct) heat transfer coefficient per unit volume
$h_g^*$ and $h_f^*$	phasic specific enthalpies of vapor and liquid associated with wall (thermal boundary layer) interface mass transfer, respectively,
i	imaginary part
<b>I</b>	Matrix of coefficients of inertial terms
<b>J</b>	Matrix of coefficients of convective terms
k	wave number
$K_f, K_g$	Isothermal Compressibility
L	length
N	number of equal control volumes in which a system is divided axially
P	Pressure
$P_s$	Saturation pressure
q	Heat flux (W/m <sup>2</sup> )
Q	volumetric heat addition rate (W/m <sup>3</sup> )
$Q_{wg}$	Gaseous phase wall heat transfer rates per unit volume
$Q_{wf}$	Liquid phase wall heat transfer rates per unit volume
$Q_{ig}$	interface heat transfer terms gaseous phase to liquid phase
$Q_{if}$	interface heat transfer terms liquid phase to gaseous phase
R	gas constant
s	second
S	slip ratio
$T_f$	fluid liquid phase temperature (K)
$T_g$	fluid vapor phase temperature (K)
$T^s$	Saturation temperature (K)
t	Time
u	specific internal energy (J/kg)
$V_f$	fluid liquid phase velocity (m/s)
$V_g$	fluid vapor phase velocity (m/s)
$V_I$	Interfacial velocity
$V_m$	Mixture velocity (m/s)
W	wall
x	spatial distance

## Greek

$\alpha$	void fraction
$\beta$	coefficient of isobaric thermal expansion ( $K^{-1}$ )
$\rho_f$	Density of liquid phase ( $kg/m^3$ )
$\rho_g$	Density of vapor phase ( $kg/m^3$ )
$\rho_m$	Density of mixture ( $kg/m^3$ )
$\Gamma$	volumetric mass exchange rate ( $kg/m^3 \cdot s$ )
$\Gamma_g$	vapor generation rate
$\Gamma_{ig}$	mass transfer at the vapor/liquid interface in the bulk fluid
$\Gamma_w$	mass transfer at the vapor/liquid interface in the thermal boundary layer near the walls
$K$	wave number
$\lambda_r$	Eigenvalues of generalized system
$\lambda$	Wavelength, length scale
$v$	Specific volume ( $m^3/kg$ )
$\omega$	angular velocity
$\rho$	density ( $kg/m^3$ )
$\epsilon$	Surface roughness
$\epsilon$	Inherent error in numerical solution
$\vec{\phi}$	Column vector of primary independent variables
$\phi$	Donor property
$\Delta t$	Finite difference time step
$\Delta x$	Finite difference space interval

## Abbreviations

1-D	one dimensional
DISS	energy dissipation function ( $W/m^3$ )
FIF, FIG	inter-phase drags coefficients (liquid, vapor) ( $s^{-1}$ )
FI	inter phase drag coefficient ( $m^3/kg \cdot s$ )
$F_{vm}$	virtual mass force
FW	First Wall
FWF, FWG	wall drag coefficients (liquid, vapor) ( $s^{-1}$ )
HLOSSF, HLOSSG	Frictional loss (fluid, steam/non-condensable) ( $m/s$ )
WCLL	Water Cool Lead-Lithium
LOCA	Loss of Coolant Accident
PWR	Pressurized Water Reactor
TFM	Two Fluid Models
UVUT	unequal velocity and unequal temperature
VISF, VISG	( $m^2/s^2$ ) analytical viscosity component in equation of motion (fluid, vapor/gas) TBS
Blanket System	Test

## Superscripts

s	saturation value
-	Vector

## Subscripts

f	liquid phase
g	vapor phase
i	inter phase
m	mixture property
min	minimum value
max	maximum value
W	wall

## References

1. S. P. Saraswat, P. Munshi, C. Allison, (2020), "Characteristics and linear stability analysis of RELAP5 Two-Fluid Model for Two-Component, Two-Phase flow", Annals of Nuclear Energy. <https://doi.org/10.1016/j.anucene.2020.107948>
2. S. P. Saraswat, P. Munshi, C. Allison, (2020), " Linear stability analysis of RELAP5 two-fluid model in Nuclear Reactor Safety Results ", Annals of nuclear energy, Vol. 149 <https://doi.org/10.1016/j.anucene.2020.107720>
3. S. P. Saraswat, P. Munshi, C. Allison, (2020), "Non-hyperbolicity Of Conservation Equations of RELAP5two fluid model In Nuclear Reactor Safety Results: Investigation and Eigenvalue

- analysis", ASME Journal of Nuclear Engineering and Radiation Science. <https://doi.org/10.1115/1.4047161>
4. Fullmer, W. D., Ransom, V. H., and Lopez, M. A., 2014b "Linear and Nonlinear Analysis of an Unstable, but Well-posed, One-dimensional TFM for Two-phase flow Based on the Inviscid Kelvin-Helmholtz Instability", Nuclear Engineering and Design, 268, pp. 173-184.
  5. Ramshaw, J., D., and Trapp, J., A., 1978, "Characteristics, Stability, and Short-Wavelength Phenomena in Two-Phase Flow Equation Systems," Nuclear Science and Engineering, 66, 1978, pp. 93-102.
  6. Ransom, V. H. and Hicks, D. L., 1984, "Hyperbolic Two-Pressure Models for Two-Phase Flow." Journal of Computational Physics. Vol. 53, pp. 124-151.
  7. Lyczkowski, R., W., Gidaspow, D., Solbrig, C., W., and Hughes, E., D., 1978, "Characteristics and Stability Analyses of Transient One-Dimensional Two-Phase Flow Equations and Their Finite Difference Approximations", NUCLEAR SCIENCE AND ENGINEERING, 66, PP. 378-396.
  8. Heinzl, Annette; Hering, Wolfgang; Konys, Jürgen; Marocco, Luca; Litfin, Karsten; Müller, Georg; Pacio, Julio; Schroer, Carsten; Stieglitz, Robert; Stoppel, Leonid; Weisenburger, Alfons; Wetzel, Thomas (2017). Liquid Metals as Efficient High-Temperature Heat-Transport Fluids. Energy Technology, (), -. doi:10.1002/ente.201600721
  9. B.F. Gromov; Yu.S. Belomitcev; E.I. Yefimov; M.P. Leonchuk; P.N. Martinov; Yu.I. Orlov; D.V. Pankratov; Yu.G. Pashkin; G.I. Toshinsky; V.V. Chekunov; B.A. Shmatko; V.S. Stepanov (1997). "Use of lead-bismuth coolant in nuclear reactors and accelerator-driven systems." ("Use of lead-bismuth coolant in nuclear reactors and accelerator-driven ..."), 173(1-3), 207–217. doi:10.1016/s0029-5493(97)00110-6
  10. X. Cheng, (2019) Thermal Hydraulics Aspects of Liquid Metal Cooled Nuclear Reactors, Woodhead Publishing, Pages185211, ISBN9780081019801, <https://doi.org/10.1016/B978-0-08-101980-1.00005-3>.
  11. IAEA 2012, liquid metal coolants for fast reactors cooled by sodium, lead, and lead-bismuth eutectic, international atomic energy agency Vienna, IAEA NUCLEAR ENERGY SERIES No. NP-T-1.6
  12. Ciurluini, Cristiano; Giannetti, Fabio; Tincani, Amelia; Del Nevo, Alessandro; Caruso, Gianfranco; Ricapito, Italo; Cismondi, Fabio (2020). Thermal-hydraulic modeling and analysis of the Water-Cooling System for the ITER Test Blanket Module. ("(PDF) Thermal-hydraulic modeling and analysis of the Water Cooling ...") ( "(PDF) Thermal-hydraulic modeling and analysis of the Water Cooling ...") Fusion Engineering and Design, 158 (), 111709–. doi: 10.1016 / j.fusengdes.2020.111709
  13. Samad Khani Moghanaki, Marica Eboli, Nicola Forgone, Daniele Martelli, Alessandro Del Nevo, Validation of SIMMER-III code for in-box LOCA of WCLL BB: Pre-test numerical analysis of Test D1.1 in LIFUS5/Mod3 facility, Fusion Engineering and Design, Volume 146, Part A, 2019, Pages 978-982, <https://doi.org/10.1016/j.fusengdes.2019.01.131>.
  14. Weisman, J. and Tentner, A., 1981, "Application of the Method of Characteristics to Solution of Nuclear Engineering Problems", Nuclear Science and Engineering, 78:1, pp. 1-29. DOI: 10.13182/NSE81-A19603
  15. Lim, H., Lee, U., Kim, K., and Lee, W., 2002, "Application of hyperbolic two fluids equations to reactor safety code", Journal of Korean nuclear society, 35, pp. 45-54.
  16. P. Satya Murthy, N.S. Dixit, T.K. Thiagarajan, N. Venkatraman, A.M. Quraishi, A. Mushtaq, Two-fluid model studies for high density two-phase liquid metal vertical flows, International Journal of Multiphase Flow, Volume 24, Issue 5, 1998, Pages 721737, [https://doi.org/10.1016/S0301-9322\(97\)00086-4](https://doi.org/10.1016/S0301-9322(97)00086-4).
  17. Usov, E. V., Lobanov, P. D., Pribaturin, N. A., Chuhno, V. I., Kutlimetov, A. E., & Svetonosov, A. I. (2017). Numerical simulation of gas volume motion during the gas injection into liquid metal coolant. ("PAPER OPEN ACCESS ...") Journal of Physics: Conference Series, 899, 032024. doi:10.1088/1742-6596/899/3/032024

18. Drew, D. A., & Lahey, R. T. (1979). "Application of general constitutive principles to the derivation of multidimensional two-phase flow equations." ("Sci-Hub | Application of general constitutive principles to the ...") *International Journal of Multiphase Flow*, 5(4), 243–264. doi:10.1016/0301-9322(79)90024-7
19. Geurst, J. A. (1991). "Virtual mass and impulse of bubble dispersions: Reply to a note by van Wijngaarden." ("Virtual mass and impulse of bubble dispersions: reply to a note by van ...") *International Journal of Multiphase Flow*, 17(6), 815–821. doi:10.1016/0301-9322(91)90059-c
20. Watanabe, T., & Kukita, Y. (1992). "The effect of the virtual mass term on the stability of the two-fluid model against perturbations." ("The Effect of the virtual mass term on the stability of the two-fluid ...") *Nuclear Engineering and Design*, 135(3), 327–340. doi:10.1016/0029-5493(92)90200-f
21. Morita, K., and Fischer E.A, 1998, "Thermodynamic properties and equations of state for fast reactor safety analysis Part I: Analytic equation-of-state model.", 183(3), 177–191.
22. Morita, K.; E.A Fischer; K Thurnay (1998). Thermodynamic properties and equations of state for fast reactor safety analysis: Part II: Properties of fast reactor materials., 183(3), 193–211. doi:10.1016/s0029-5493(98)00176-9
23. W. R. Bohl, E. A. Fischer, L. Goutagny, P. Maudlin, H. Ninokata, F. R. Parker, D. Wilhelm, 1994, "An Advanced Fluid-Dynamics Model Volume VI: EOS-AFDM Interface", Kernforschungszentrum Karlsruhe, Postfach 3640, D-7500 Karlsruhe 1, GERMANY, January 1994.
24. Schulz, B. (1991). Thermophysical properties of the Li (17) Pb (83) alloy. *Fusion Engineering and Design*, 14(3-4), 199–205. doi:10.1016/0920-3796(91)90002-8
25. Khanna, K. N., & Khandelwal, D. P. (1981). Thermodynamic Properties of Liquid Metals and Alloys. *Physica Status Solidi (b)*, 106(2), 715–721. doi:10.1002/pssb.2221060238
26. Martelli, D., Venturini, A., & Utili, M. (2019). Literature review of lead-lithium thermophysical properties. *Fusion Engineering and Design*, 138, 183–195. doi: 10.1016/j.fusengdes.2018.11.0
27. Kasselmann, P.M., Bykov, A.Y. & Inshakov, S.A. Thermodynamic properties of liquid metals and alloys. ("Thermodynamic properties of liquid metals and alloys") *Journal of Engineering Physics* 59, 1455–1462 (1990). <https://doi.org/10.1007/BF00872967>
28. Mas de les Valls, E., Sedano, L. A., Batet, L., Ricapito, I., Aiello, A., Gastaldi, O., & Gabriel, F. (2008). ("Mas de les Valls, E., Sedano, L.A., Batet, L., Ricapito, I., Aiello, A ...") Lead–lithium eutectic material database for nuclear fusion technology. *Journal of Nuclear Materials*, 376(3), 353–357. doi: 10.1016/j.jnucmat.2008.02.016
29. Barone, G., Martelli, D., & Forgone, N. (2019). Implementation of Lead-Lithium as working fluid in RELAP5/Mod3.3. *Fusion Engineering and Design*. doi: 10.1016/j.fusengdes.2019.02.0
30. Malang, S., & Mattas, R. (1995). Comparison of lithium and the eutectic lead-lithium alloy, two candidate liquid metal breeder materials for self-cooled blankets. *Fusion Engineering and Design*, 27, 399–406. doi:10.1016/0920-3796(95)90151-5
31. Coen, V. (1985). Lithium-lead eutectic as breeding material in fusion reactors. *Journal of Nuclear Materials*, 133-134, 46–51. doi:10.1016/0022-3115(85)90110-2

32. A. Del Nevo, E. Martelli, P. Agostini, P. Arena, G. Bongiovì, G. Caruso, G. Di Gironimo, P.A. Di Maio, M. Eboli, R. Giammusso, F. Giannetti, A. Giovinazzi, G. Mariano, F. Moro, R. Mozzillo, A. Tassone, D. Rozzia, A. Tarallo, M. Tarantino, M. Utili, R. Villari, WCLL breeding blanket design and integration for DEMO 2015: status and perspectives, *Fusion Engineering and Design*, Volume 124, 2017, Pages 682-686, <https://doi.org/10.1016/j.fusengdes.2017.03.020>. (<https://www.sciencedirect.com/science/article/pii/S0920379617302235>)
33. Mozzillo, R., Del Nevo, A., Martelli, E., & Di Gironimo, G. (2017). Rationale and method for design of DEMO WCLL breeding blanket poloidal segmentation. *Fusion Engineering and Design*, 124, 664-668.
34. Di Maio, P. A., Arena, P., Bongiovì, G., Chiovaro, P., Forte, R., & Garitta, S. (2016). On the optimization of the first wall of the DEMO water-cooled lithium lead outboard breeding blanket equatorial module. *Fusion Engineering and Design*, 109, 335-341.
35. Martelli, E., Caruso, G., Giannetti, F., Giovinazzi, A., & Del Nevo, A. (2017). CFD analysis of WCLL BB PbLi manifold. *Fusion Engineering and Design*, 124, 1015-1018.